Contents lists available at SciOpen

Food Science and Human Wellness

journal homepage: https://www.sciopen.com/journal/2097-0765

China Food Publishing Co.

# *Atractylodes macrocephala* water extract exerts a protective effect against high fat and high sugar diet-induced NAFLD by inhibiting the TRAF1/ASK1/JNK pathway

Kejian Wei[a,b,1], Binhui Pan[a,1], Jing Liu[a,1], Wenlong Zhang[a], Jie Su[a], Hengpu Zhou[a], Zimo Dong[a], Jingjing Yu[a,*], Suhong Chen[a,*], Guiyuan Lyu[a,*]

[a] *School of Pharmaceutical Sciences, Zhejiang Chinese Medical University, Hangzhou 310053, China*
[b] *Wuxi School of Medicine, Jiangnan University, Wuxi 214122, China*

ARTICLE INFO

*Article history:*
Received 29 July 2024
Received in revised form 28 August 2024
Accepted 21 January 2025

*Keywords:*
*Atractylodes macrocephala*
High-sugar and high-fat diet
Non-alcoholic fatty liver disease
Inflammation
Apoptosis
TRAF1/ASK1/JNK

ABSTRACT

Non-alcoholic fatty liver disease (NAFLD) has emerged as a global health issue, making early prevention and treatment are crucial. *Atractylodes macrocephala*, as a functional food, holds potential in improving liver metabolic diseases. The aim of this study was to investigate whether *A. macrocephala* water extract (AMW) has a preventive effect on NAFLD induced by high-fat, high-sugar (HSHF) diet. Initially, the components of AMW were analyzed, revealing the high content of polysaccharides and lactones as its main constituents. Mice were then subjected to HSHF diet and administered AMW for 12 weeks to observe its effects on glucose and lipid metabolism, hepatic lipid accumulation, oxidative damage, inflammatory injury, and apoptosis. The results indicated that AMW significantly improved glucose and lipid metabolism disorders in mice, reduced hepatic lipid accumulation, oxidative damage, and inflammatory injury. Specifically, AMW notably decreased the release of tumor necrosis factor-alpha (TNF-α), thereby inhibiting the activation of the hepatic TRAF1/ASK1/JNK pathway, which alleviated the progression of inflammatory responses. Additionally, c-Jun N-terminal kinase (JNK) phosphorylation was reduced, inhibiting the activation of downstream factor activates protein kinase B (AKT), which in turn led to decreased expression of apoptosis-related factors such as Bcl-2-associated X protein (Bax), cytochrome C (Cyt C), and Cleaved Caspase-3, while increasing B-cell lymphoma-2 (Bcl-2) expression. These findings suggest that AMW may protect against HSHF-induced NAFLD by reducing hepatic oxidative damage, inhibiting inflammation, and preventing apoptosis, potentially through inhibition of the TRAF1/ASK1/JNK pathway.

© 2026 Beijing Academy of Food Sciences. Publishing services by Tsinghua University Press.
This is an open access article under the CC BY-NC-ND license
(http://creativecommons.org/licenses/by-nc-nd/4.0/).

## 1. Introduction

Non-alcoholic fatty liver disease (NAFLD) is a common metabolic disorder that currently affects approximately one-quarter of the global adult population's health[1-2]. Modern research indicates that NAFLD encompasses non-alcoholic fatty liver (NAFL) and non-alcoholic steatohepatitis (NASH), and its development is closely related to long-term high-sugar, high-fat dietary habits[3]. Such diets can disrupt hepatic glucose and lipid metabolism, leading to lipid accumulation in the liver, liver damage, apoptosis, and subsequent fibrosis, which may further progress to cirrhosis or hepatocellular carcinoma[4-6]. Thus, early prevention and treatment of NAFLD are particularly critical in clinical practice.

[1] These authors contributed equally to this work.

* Corresponding authors at: School of Pharmaceutical Sciences, Zhejiang Chinese Medical University, Hangzhou 310053, China.
*E-mail address*: zjtcmlgy@163.com (G.Y. Lyu); chensuhong@zjut.edu.cn (S.H. Chen); Yujingjing8223@163.com (J.J. Yu)

Peer review under responsibility of Beijing Academy of Food Sciences.

SciOpen Publishing services by Tsinghua University Press

http://doi.org/10.26599/FSHW.2025.9250527

2213-4530/© 2026 Beijing Academy of Food Sciences. Publishing services by Tsinghua University Press. This is an open access article under the CC BY-NC-ND license (http://creativecommons.org/licenses/by-nc-nd/4.0/).

The pathogenesis of NAFLD is complex and multifaceted. Oxidative stress and inflammation are currently recognized as major mechanisms of NAFLD onset[7-8]. Research has shown that glucose and lipid metabolism disorders in NAFLD patients lead to excessive production of reactive oxygen species (ROS), inducing oxidative stress, lipid peroxidation, and oxidative damage[9-11]. ROS-induced oxidative damage further promotes the overproduction of inflammatory factors, such as tumor necrosis factor-alpha (TNF-α), triggering inflammatory responses and causing inflammatory injury[12]. Excessive TNF-α release enhances the production of tumor necrosis factor receptor-associated factor 1 (TRAF1), which phosphorylates apoptosis signal-regulating kinase 1 (ASK1) and activates downstream factors such as c-Jun N-terminal kinase (JNK). Persistent JNK activation, on one hand, causes massive production of inflammatory factors, exacerbating inflammatory injury[13-15], and on the other hand, activates protein kinase B (AKT), modulating apoptosis-related proteins such as B-cell lymphoma-2 (Bcl-2) and Bcl-2-associated X protein (Bax), ultimately promoting cell apoptosis and worsening liver damage[16-18]. Therefore, it may be possible to improve NAFLD by regulating glucose and lipid metabolism disorders, suppressing excessive hepatic oxidative stress, and targeting the TRAF1/ASK1/JNK signaling pathway.

Modern research has demonstrated that certain natural products or foods have beneficial effects on regulating glucose and lipid metabolism, mitigating cellular damage, and protecting the liver[19-21]. *Atractylodes*, a perennial herbaceous plant of the Asteraceae family, is widely cultivated in East Asia and has been used as a "dual-purpose" medicinal and dietary product for centuries[22-23]. It has been officially approved as a functional food by the National Health Commission of the People's Republic of China[24]. As a natural plant, *Atractylodes* contains a complex composition, primarily including volatile oils, polysaccharides, and lactones[25-27]. Some studies have demonstrated that *Atractylodes* exhibits significant pharmacological effects on lipid metabolism regulation, liver protection, and reducing hepatic cell apoptosis, potentially due to the antioxidative and anti-inflammatory activities of its lactones and polysaccharides[28-29]. Modern studies suggest that *Atractylodes* decoction has a potential ameliorative effect on liver damage induced by NAFLD, but the specific therapeutic effects and mechanisms require further clarification. Some researchers have found that *Atractylodes* can reduce cell apoptosis by inhibiting excessive activation of the JNK pathway in certain diseases[30-31]. However, whether Atractylodes can prevent NAFLD through JNK pathway inhibition has not been conclusively studied. Furthermore, traditional Chinese medicine often employs water decoctions of *Atractylodes* to treat digestive disorders, suggesting that the active components in its water extract may be the foundation of its therapeutic properties.

This study established a mouse model of NAFLD induced by high-fat and high-sugar diet (HSHF) and evaluated the preventive effects of *Atractylodes macrocephala* water extract (AMW). The study also explored the relevant mechanisms of action based on the TRAF1/ASK1/JNK signaling pathway.

## 2. Materials and methods

### 2.1 Reagents and materials

High sugar and high fat diet (composed of 20% carbohydrates, 15% fat, 0.8% cholesterol, 0.2% sodium cholate, appropriate amounts of casein, calcium hydrogen phosphate, and calcium carbonate) was purchased from Trophic Animal Feed High-Tech Co., Ltd. (Nantong, China).

Kits for total cholesterol (TC), triglyceride (TG), low-density lipoprotein cholesterol (LDL-C) were all purchased from Medicalsystem Biotechnology Co., Ltd. (Zhejiang, China). Kits for liver pyruvate, lactic acid (LD), lactate dehydrogenase (LDH), glycogen, superoxide dismutase (SOD), malondialdehyde (MDA), free fatty acid (FFA), TC, TG, glucose, aspartate aminotransferase (AST), alanine aminotransferase (ALT), alkaline phosphatase (ALP), γ-glutamyl transpeptidase (γ-GT) were all purchased from NJJCBIO (Nanjing, China). Enzyme-linked immunosorbent assay (ELISA) kits for lipid peroxide (LPO), 4-hydroxynonenal (4-HNE) were all purchased from Quanzhou Ruixin Biotechnology Co., Ltd. (Quanzhou, China). ELISA kits for leptin (LEP), chemerin (CHEM), adiponectin (ADPN), secreted frizzled related protein 5 (SFRP5), insulin, interleukin-1β (IL-1β), interleukin-6 (IL-6), TNF-α were all purchased from Jiangsu Meimian Industrial Co., Ltd. (Yancheng, China).

Anti-rabbit myeloid differentiation factor 88 (MyD88) was purchased from Affinity Biosciences (Changzhou, China). Anti-rabbit TNF-α was purchased from Ruiying Biotechnology Co.(Suzhou, China). Anti-rabbit insulin receptor substrate 2 (IRS2), phosphorylated IRS2 (p-IRS2), Bcl-2, cytochrome C (Cyt C) were all purchased from Abcam (Cambridge, UK). Anti-rabbit Toll-like receptor 4 (TLR4), anti-mouse Bax, IL-1β, ASK1 were all purchased from Proteintech (Wuhan, China). Anti-rabbit glucose transporter 2 (GLUT2), p-ASK1, JNK, AKT, p-AKT were all purchased from Zen-bio (Chengdu, China). Anti-rabbit p-JNK, cleaved cysteinyl aspartate specific proteinase 3 (Cleaved Caspase-3) were all purchased from Cell Signaling Technology (Massachusetts, USA). Anti-rabbit TRAF1, IL-6, horseradish peroxidase-conjugated anti-rabbit and anti-mouse IgG secondary antibodies were all purchased from HUABIO (Hangzhou, China).

### 2.2 Preparation of AMW and ezetimibe water solution

Test drug: took 500 g of *A. macrocephala* (Zhejiang Qianwang Traditional Chinese Medicine Co., Ltd., Hangzhou, China) (Fig. 1A) powder, added 20 times the amount of pure water, and extracted it 3 times, boiling for 2, 1, and 1 h, respectively. Combined the decoctions from the 3 extractions, concentrated under reduced pressure to 1 g of raw medicine per mL, and then used pure water to adjust the concentration of AMW to 0.2 and 0.1 g/mL (Fig. 1B). Stored in a refrigerator at 4 ℃ for later use.

Positive control drug: took 100 mg ezetimibe tablets (Hangzhou Merck Sharp & Dohme Pharmaceuticals Co., Ltd., Hangzhou China), and prepared a 0.1 mg/mL ezetimibe water solution using pure water. Stored in a refrigerator at 4 ℃ for later use.

### 2.3 Experimental animals

A total of 40 male ICR mice (6−8 weeks, SPF grade) were purchased from the Laboratory Animal Business Department of the Shanghai Institute of Planned Parenthood Research. All animals were housed at an ambient temperature ((22 ± 2) ℃) and humidity ((55 ± 15)%) with a 12 h light/dark cycle. All animal procedures were performed in accordance with the Guidelines for Laboratory Animal Management and Ethics Committee of Zhejiang University of Traditional Chinese Medicine (approval number: IACUC-20230918-28).

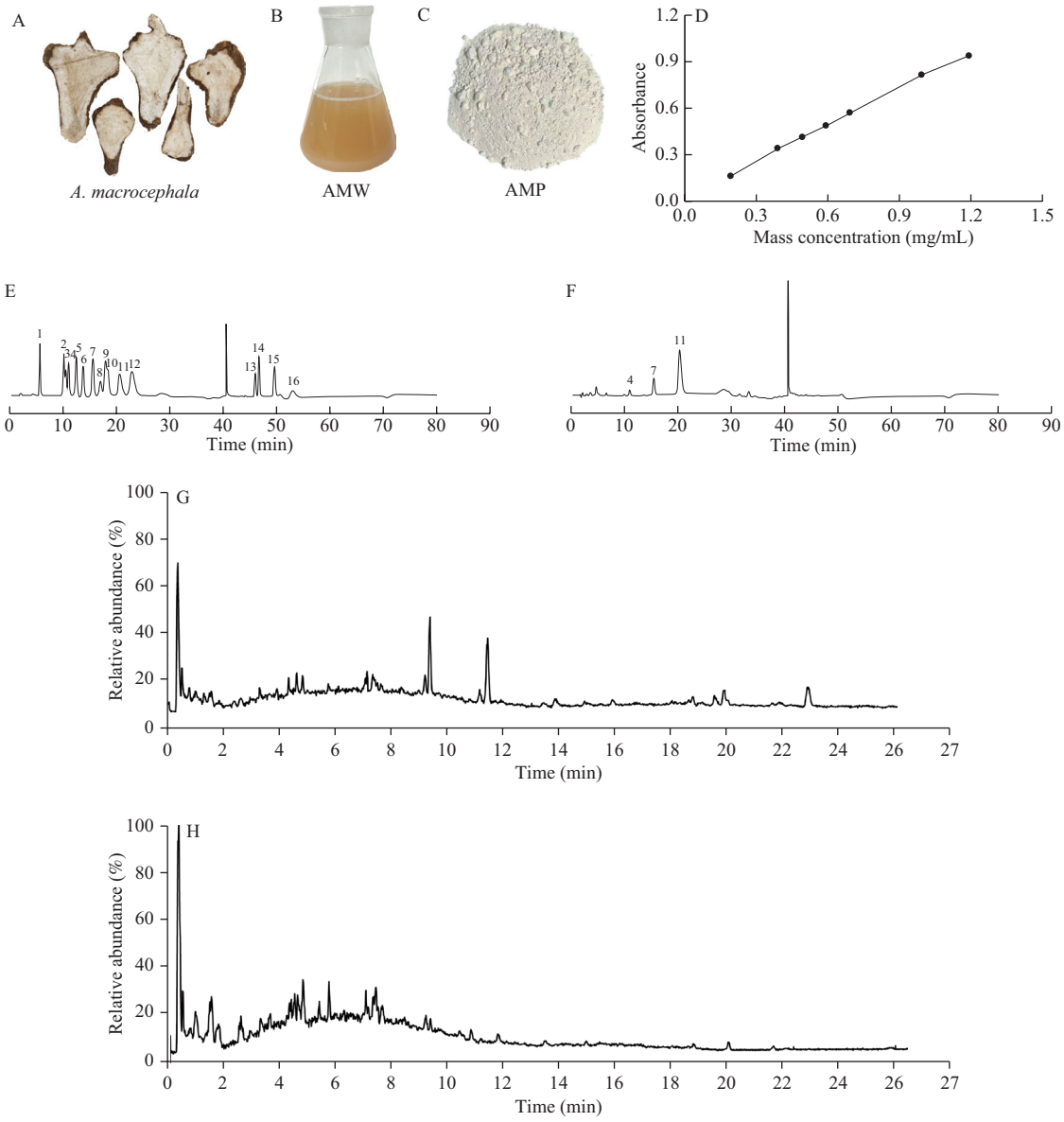



**Fig. 1** Experimental drug samples and component analysis. (A) *A. macrocephala*. (B) AMW. (C) AMP. (D) Glucose mass concentration standard curve. Monosaccharide composition analysis: (E) standards; (F) AMP. Total ion flow diagram of AMW: (G) positive ion mode; (H) negative ion mode.

### *2.4 Experimental protocol*

#### *2.4.1 AMW component assay*

Weighed 10 g *A. macrocephala* powder, added 200 mL pure water, and repeated the decoction process as in Section 2.2 for AMW extract, finally concentrating it to 10 mL, then added ethanol to 80% ethanol concentration and refrigerate overnight to precipitate polysaccharides. Removed the supernatant and dissolved the precipitate in water, added 1/4 volume of Sevage reagent (chloroform:butanol = 4:1), then shook for 10 min. Centrifuge at 3 500 r/min for 10 min, carefully extracted the upper polysaccharide solution, removed the organic phase and precipitation, and repeated the above process 6 times to collect the solution. The polysaccharide solution was evaporated to concentrate it, and then freeze-dried to obtain 989 mg *A. macrocephala* polysaccharide (AMP) lyophilized powder (Fig. 1C).

Accurately weighed 8.50 mg AMP freeze-dried powder and diluted it with 100 mL pure water to prepare the 0.085 mg/mL test solution. Weighed 25.00 mg *D*-glucose and diluted it with pure water to prepare the 0.1 mg/mL reference solution. Took 0.2, 0.4, 0.6, 0.8, 1.0, 1.2 mL of the reference solution to the 10 mL stoppered test tube respectively and then added water to make up to 2.0 mL. Carefully added 1.0 mL freshly prepared 5% phenol solution, shook well, then added 5.0 mL concentrated sulfuric acid in an ice bath, shook well, cooled for 5 min, then placed in a boiling water bath for 20 min. Afterward, cooled it in an ice bath for 5 min. Preheated the UV spectrophotometer 0.5 h in advance, using the corresponding reagent as blank, and measured the absorbance (486 nm) to draw the standard curve. Similarly, in the 10 mL stoppered test tube, took 1.0 mL the test solution, added 1 mL pure water, shook well, prepared 3 parallel sample solutions and repeated the steps of the reference operation. Measured the absorbance to calculate the content of AMP.

Accurately weighed a suitable amount of 16 monosaccharide standards (fucose, rhamnose, arabinose, galactose, glucose, xylose, mannose, fructose, ribose, galacturonic acid, glucuronic acid, glucosamine hydrochloride, galactosamine hydrochloride, *N*-acetyl-*D*-glucosamine, guluronic acid, mannuronic acid). Added 2 mL 3 mol/L trifluoroacetic acid (TFA) to each, and hydrolyzed at 80 ℃ for 2 h. Afterward, evaporated the TFA under a nitrogen stream until dry. Reconstituted the residue in deionized water, vortexed thoroughly, and prepared standard stock solutions. For sample, precisely weighed 5 mg into an ampoule. Added 2 mL of 3 mol/L TFA and hydrolyzed at 80 ℃ for 2 h. Transfer the hydrolyzed solution to a centrifuge tube, dried under a nitrogen stream, then added 5 mL water, and vortexed thoroughly. Diluted 50 μL sample solution with 950 μL deionized water, centrifuged at 12 000 r/min for 5 min. Used a Dionex Carbopac™ PA20 column (3 mm × 150 mm, 6.0 μm). The mobile phases were as follows: A, water; B, 15 mmol/L NaOH; C, 15 mmol/L NaOH with 100 mmol/L sodium acetate. The flow rate was set at 0.3 mL/min, with an injection volume of 25 μL. The column temperature was maintained at 30 ℃, and the elution gradient was programmed as follows: 0 min A/B/C (98.8:1.2:0), 18 min A/B/C (98.8:1.2:0), 20 min A/B/C (50:50:0), 30 min A/B/C (50:50:0), 30.1 min A/B/C (0:0:100), 46 min A/B/C (0:0:100), 46.1 min A/B/C (0:100:0), 50 min A/B/C (0:100:0), 50.1 min A/B/C (98.8:1.2:0), 80 min A/B/C (98.8:1.2:0).

A solution of AMW at a concentration of 1 g/mL was placed in a 60 mL separatory funnel and extracted 3 with equal volumes of water-saturated *n*-butanol. The *n*-butanol fractions were collected, dried, and the resultant dry solid was dissolved in methanol to a concentration of 5 mg/mL for mass spectrometry analysis. The chromatographic conditions were as follows: ACQUITY UPLC BEH $C_{18}$ column (2.1 mm × 50 mm, 1.7 μm); mobile phase consisting of acetonitrile (A) and 0.1% formic acid solution (B), gradient elution: 10%−48% A (0−8 min), 48%−50% A (8−12 min), 50%−70% A (12−16 min), 70%−80% A (16−18 min), and 80% A (18−26 min); flow rate of 0.2 mL/min; detection wavelength of 330 nm; column temperature maintained at 25 ℃. Mass spectrometry conditions included both positive and negative ion modes using an electrospray ionization (ESI) source; ion source temperature set at 550 ℃; curtain gas at 35 psi; collision-activated dissociation (CAD) gas at 8 psi; ion source gases 1 and 2 both at 55 psi; spray voltage at 5.5 kV. Scanning modes included TOF MS from *m/z* 50−1 500 and TOF MS/MS from *m/z* 30−1 500. Data was collected by Sciex OS 3.0.0.3339 workstation, and data was processed by the Explorer and Analytics modules of the Sciex OS 3.0.0.3339 software. The final results were obtained after comparative analysis.

### 2.4.2 *Establishment and grouping of animal models*

After a week of acclimation, 40 ICR mice were randomly divided into 5 groups based on their body weight. The groups included control group (Control), model group (HSHF), EZB group (Ezetimibe at 1 mg/kg), low-dose AMW group (AMW_L at 1 g/kg), and high-dose AMW group (AMW_H at 2 g/kg). Except for the Control group, which was fed a standard diet, the remaining groups were fed HSHF daily. Concurrent with model induction, the treatment groups were orally administered their respective drugs, while the control and model groups received distilled water, all the above groups were intraliver at a volume of 0.1 mL/10 g once daily for a continuous 12 weeks. During the experimental period, the mice were weighed biweekly. At the end of the 12-week experiment, the mice were sacrificed by cervical dislocation after orbital blood collection, and then dissected to rapidly excise and weighed the wet liver (Fig. 2A). The liver index was calculated using the following formula:

$$\text{Liver index (\%)} = \frac{\text{Liver wet weight (g)}}{\text{Body weight (g)}} \times 100 \quad (1)$$

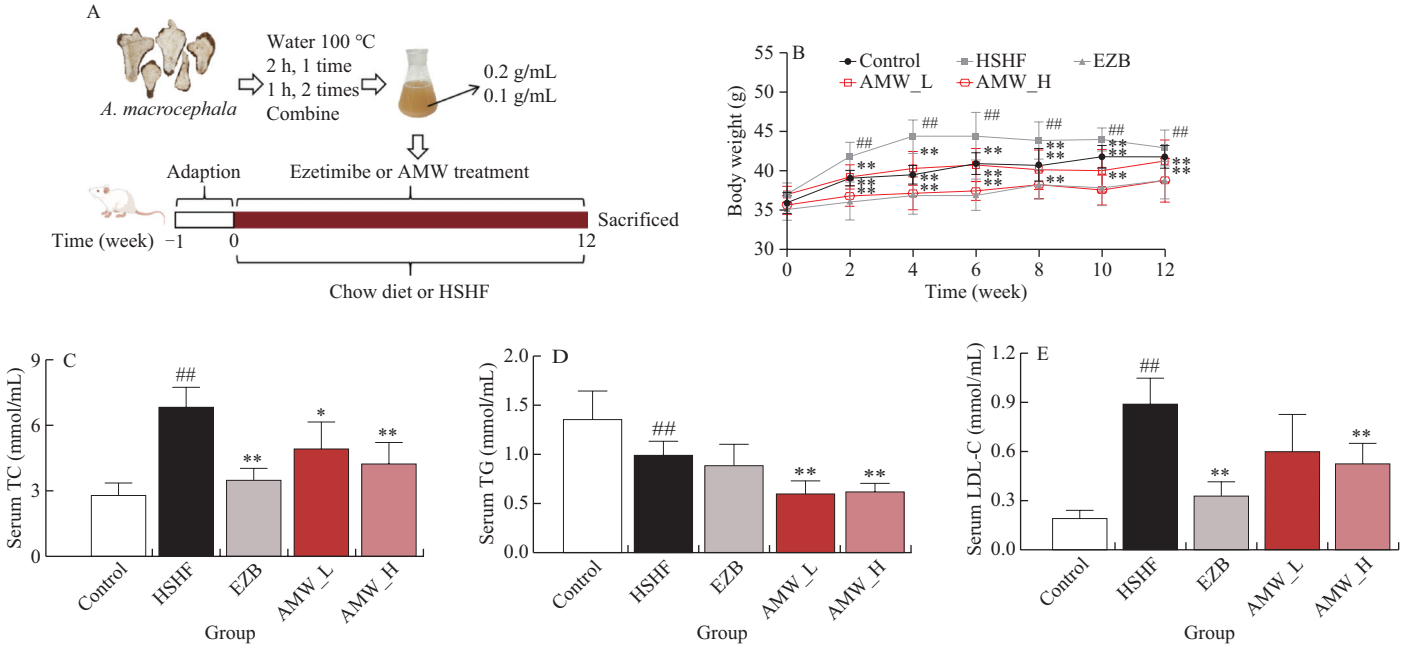



**Fig. 2** Experimental flowchart and the impact of AMW on lipid metabolism. (A) Experimental flowchart. (B) Body weight changes. Serum levels of (C) TC, (D) TG, (E) LDL-C ($n$ = 8). (F) H&E and Oil Red O staining of liver sections (200×, scale bar = 100 μm). (G) Liver wet weight. (H) Liver coefficient. Liver levels of (I) TC, (J) TG ($n$ = 8). The data were expressed as means ± SD. $^{\#\#}P < 0.01$ compared with the Control group; $^{*}P < 0.05$, $^{**}P < 0.01$ compared with the HSHF group.

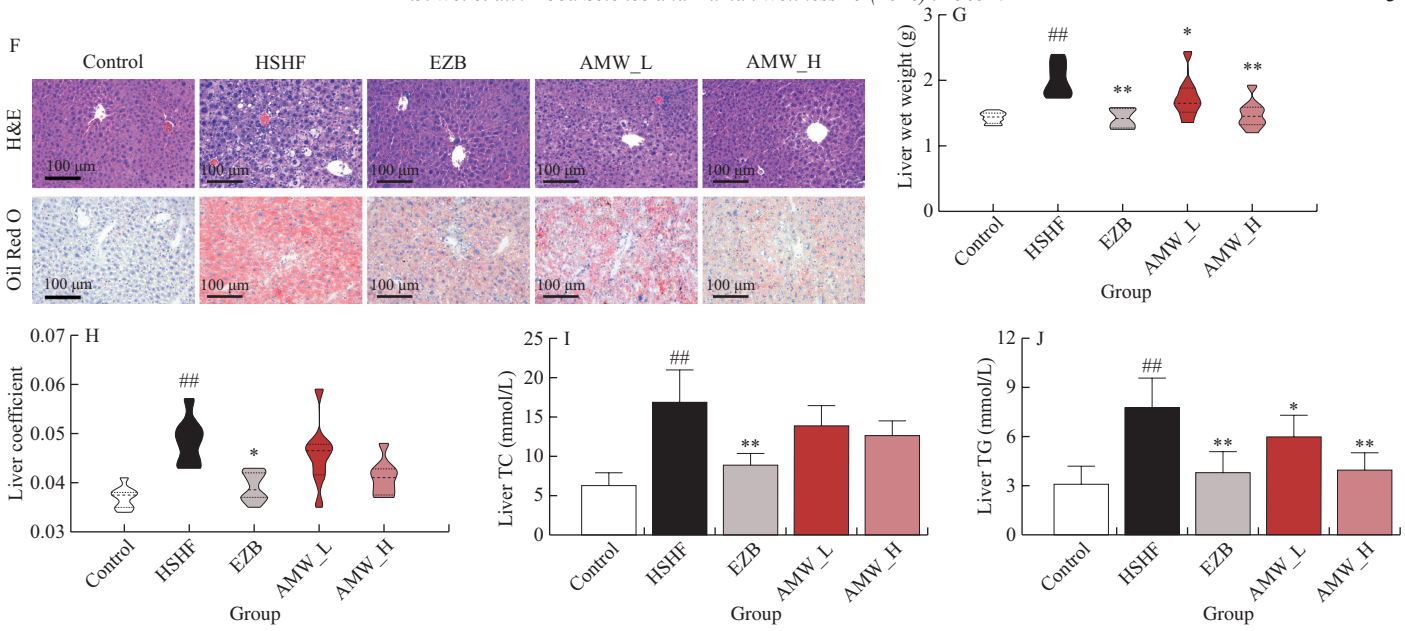



**Fig. 2** (*Continued*)

### 2.4.3 *Oral glucose tolerance test (OGTT)*

After fasting for 12 h, blood was collected from the tail tip of the mice to determine fasting blood glucose (FBG) levels. Then, glucose was administered *via* oral gavage at 0.1 mL/10 g, and blood glucose levels were measured at 5, 10, 30, 60, and 120 min post-administration. After completing the test, an OGTT curve was plotted with time on the *x*-axis and blood glucose concentration on the *y*-axis, and the area under the curve (AUC) was calculated.

### 2.4.4 *Biochemical analysis*

Blood samples were collected and centrifuged at 3 500 r/min for 10 min to obtain the serum, which was used to determine the levels of TC, TG, LDL-C, glucose.

Liver tissues were collected and homogenized in a ratio of 1:9 (mg/μL) of ice-cold anhydrous ethanol using a homogenizer. The homogenate was then centrifuged at 12 000 r/min for 15 min, and the supernatant was collected to measure the levels of TC and TG in the liver. Following the same procedure but using ice-cold saline for grinding and centrifugation, the resultant supernatant was used to measure liver levels of AST, ALT, ALP, γ-GT, pyruvate, LD, LDH, liver glycogen, SOD, and MDA.

### 2.4.5 *ELISA*

The contents of insulin, LEP, CHEM, ADPN, and SFRP5 in the serum sample and the contents of LPO, 4-HNE, IL-1β, IL-6, and TNF-α in the liver homogenate sample were determined using ELISA method.

### 2.4.6 *Insulin resistance evaluation*

After measuring FBG and fasting insulin (FINS), the insulin resistance index (IR) and the insulin sensitivity index (IS) were calculated using the homeostasis model assessment method. The calculation formulas were as follows:

$$IR = \frac{(FPG \times FINS)}{22.5} \quad (2)$$

$$IS = \ln(1/(FPG \times FINS)) \quad (3)$$

### 2.4.7 *Histopathological analysis*

The liver tissues were fixed in formalin solution for 48 h, followed by dehydration and embedding in paraffin. Sections of 4 μm thickness were cut for histological evaluation using hematoxylin and eosin (H&E) staining and Masson's trichrome staining (G1346, Solarbio, Beijing, China) for analyzing the extent of liver fibrosis. Additionally, 8 μm cryosections from the same region of the liver were stained with Oil Red O (G1261, Solarbio, Beijing, China) to analyze hepatic lipid deposition.

### 2.4.8 *ROS assay*

Removed the liver frozen sections from the −20 °C freezer and rewarmed them to room temperature. Fixed in methanol for 10 min, allowed the methanol to dry slightly, then placed in a 37 °C oven for 15 min. Then, washed the sections 3 times in PBS (pH 7.4) on a decolorizing shaker, 5 min each time. After the sections were slightly dried, added dihydroethidium staining solution (Shanghai Aladdin Biochemical Technology Co., Ltd., Shanghai, China) at a concentration of 1:1 000, incubate in a light-proof incubator at 37 °C for 30 min, then wash the sections 3 times in PBS (pH 7.4) on a decolorizing shaker, 5 min each time. After the sections were slightly dried, add 4′,6-diamidino-2-phenylindole (DAPI) nuclear staining solution, incubate in the dark at room temperature for 10 min, then wash the sections 3 times in PBS (pH 7.4) on a decolorizing shaker, 5 min each time. After the sections were slightly dried, seal the sections with an anti-fluorescence quenching mounting medium. The sections were observed under AXIO SCOPE.A1 Zeiss upright fluorescence microscope (ZEISS, Germany).

### 2.4.9 *TUNEL assay*

Paraffin sections of liver tissue (4 μm) were taken and processed according to the TUNEL assay kit (Shanghai Recordbio Biological

Technology, Shanghai, China) instructions. After sealing the sections with anti-fluorescence quenching mounting medium, they were observed under AXIO SCOPE.A1 Zeiss upright fluorescence microscope (ZEISS, Germany).

#### 2.4.10 Immunofluorescence analysis

Paraffin sections of liver tissue (4 μm) were prepared by dewaxing, antigen retrieval, and blocking, followed by the addition of antibodies for Bax, Bcl-2, Cleaved Caspase-3, and incubated overnight at 4 ℃. Secondary antibodies were added in the dark and incubated at 37 ℃ for 30 min. After nuclear staining with DAPI, the sections were sealed with antifade mounting medium and the levels of Bax, Bcl-2, and Cleaved Caspase-3 in the liver tissue were observed under AXIO SCOPE.A1 Zeiss upright fluorescence microscope (ZEISS, Germany).

#### 2.4.11 Immunohistochemistry analysis

Paraffin sections of liver tissue (4 μm) were processed to eliminate endogenous peroxidase activity, undergo antigen retrieval, and be blocked with BSA. Then, antibodies for IL-6, IL-1β, TNF-α, MyD88, and TLR4 were applied and incubated overnight at 4 ℃. Secondary antibodies were added and incubated at 37 ℃ for 30 min. After 3,3′-diaminobenzidine (DAB) development, hematoxylin staining, ethanol dehydration, and sealing with neutral resin, the levels of IL-6, IL-1β, TNF-α, MyD88, and TLR4 proteins were observed under MF43-N upright fluorescence microscope (Micro-shot Technology Co., Ltd., Guangzhou, China) and analyzed using ImageJ software.

#### 2.4.12 Western blot analysis

Liver tissue was thoroughly ground by SCIENTZ-48 High-Throughput Tissue Grinder (Ningbo Xinzhi Biotechnology Co., Ltd., Ningbo, China), then an appropriate amount of RIPA lysis buffer was added, and the mixture was left on ice for 10 min. After centrifugation, the supernatant was collected to extract tissue protein. The protein concentration was determined by the BCA method, and the protein samples were subjected to sodium dodecyl sulfate-polyacrylamide gel electrophoresis, then transferred to a PVDF membrane. The membrane was blocked with BSA for 1.5 h, followed by the addition of antibodies for IRS2, p-IRS2, GLUT2, TNF-α, TRAF1, ASK1, p-ASK1, JNK, p-JNK, AKT, p-AKT, Bax, Bcl-2, Cyt C, Cleaved Caspase 3, and incubated overnight at 4 ℃. The membrane was washed 3 times with TBST, 15 min each time; secondary antibodies were added, and incubated at room temperature for 2 h; followed by 3 more TBST washes, 15 min each time. ECL chemiluminescent substrate was then added, and protein bands were detected using a Modena gel imaging system and analyzed with ImageJ software.

#### 2.4.13 Statistical analysis

All data were presented as means ± SD of at least 3 individual experiments. The results were statistically analyzed by one-way ANOVA using SPSS Statistical 26 Software (IBM, USA). Statistical significance was determined as $P < 0.05$, and highly statistical significance was determined as $P < 0.01$, with different alphabetical letters applied in all histograms, indicating significant differences between the groups.

## 3. Results

### 3.1 Analysis of the components of AMW

Using *D*-glucose as the standard, with the mass concentration plotted on the *x*-axis and absorbance on the *y*-axis, a linear regression equation of $y = 0.779\ 7x + 0.029\ 6$ ($R^2 = 0.998$) (Fig. 1D) was established. Based on this, the content of AMP in the AMW lyophilized powder was calculated to be 80.87%. Upon comparison with monosaccharide reference substances, it was determined that the polysaccharides from *A. macrocephala* primarily consist of Ara (6.36 μg/mg), Glc (20.89 μg/mg), and Fru (291.72 μg/mg) (Figs. 1E-F and Table 1).

**Table 1**
AMP composition summary.

| No. | Compound | Area | Retention time (min) | Concentration (μg/mg) |
|---|---|---|---|---|
| 1 | Fuc | 0 | 5.634 | 0.00 |
| 2 | GalN | 0 | 10.125 | 0.00 |
| 3 | Rha | 0 | 10.509 | 0.00 |
| 4 | Ara | 2.63 | 10.975 | 6.36 |
| 5 | GlcN | 0 | 12.467 | 0.00 |
| 6 | Gal | 0 | 13.750 | 0.00 |
| 7 | Glc | 9.92 | 15.475 | 20.89 |
| 8 | GlcNAc | 0 | 17.009 | 0.00 |
| 9 | Xyl | 0 | 17.959 | 0.00 |
| 10 | Man | 0 | 18.342 | 0.00 |
| 11 | Fru | 42.529 | 20.325 | 291.72 |
| 12 | Rib | 0 | 22.917 | 0.00 |
| 13 | GalA | 0 | 45.984 | 0.00 |
| 14 | GulA | 0 | 46.709 | 0.00 |
| 15 | GlcA | 0 | 49.600 | 0.00 |
| 16 | ManA | 0 | 53.017 | 0.00 |

After mass spectrometric analysis of the AMW, 31 compounds were identified in the positive and negative ion mode, primarily consisting of flavonoids and sesquiterpenes (Figs. 1G-H and Table 2). The identification was confirmed by comparing the *m/z*, secondary fragment ions, and compound cleavage patterns in the mass spectral data, validating our expectations.

### 3.2 Impact of AMW on lipid metabolism in NAFLD mice

Throughout the experimental period, body weight measurements indicated that mice in the HSHF group weighed more than those in the Control group ($P < 0.01$) (Fig. 2B); starting from the second week, weight gain in all AMW groups was significantly reduced compared to the HSHF group ($P < 0.01$) (Fig. 2B). The impact of AMW on lipid metabolism was assessed by measuring TC, TG, and LDL-C. Compared to the Control group, the HSHF group showed elevated levels of serum TC and LDL-C ($P < 0.01$) (Figs. 2C-E); however, levels of serum TC and TG in the AMW_L and AMW_H groups and levels of serum LDL-C in the AMW_H group were reduced to varying extents ($P < 0.01$ or $P < 0.05$) (Figs. 2C-E).

**Table 2**
AMW composition summary.

| No. | Compound | Retention time (min) | Adduction | Molecular formula | Theoretical mass (*m/z*) | MS/MS (*m/z*) | Identification |
|---|---|---|---|---|---|---|---|
| 1 | *cis*-Aconitic acid | 0.46 | $[M-H]^-$ | $C_6H_6O_6$ | 173.009 | 131.083 4, 112.085 7 | Aliphatic organic acids |
| 2 | Citric acid | 0.58 | $[M-H]^-$ | $C_6H_8O_7$ | 191.020 | 111.010 4, 85.031 1, 67.020 1, 57.035 7 | Aliphatic organic acids |
| 3 | Chlorogenic acid | 1.59 | $[M-H]^-$ | $C_{16}H1_8O_9$ | 353.088 | 191.063 0, 179.035 8, 173.046 7, 161.025 5, 135.045 9, 127.040 6, 85.030 5 | Aromatic organic acids |
| 4 | Quinic acid | 1.60 | $[M-H]^-$ | $C_7H_{12}O_6$ | 191.056 | 145.456 5, 109.029 9, 93.035 5, 85.029 6, 59.013 8 | Aliphatic organic acids |
| 5 | Caffeic acid | 2.28 | $[M-H]^-$ | $C_9H_8O_4$ | 179.035 | 135.047 5 | Aromatic organic acids |
| 6 | Icariside D1 | 3.45 | $[M-H]^-$ | $C_{19}H_{28}O_{10}$ | 415.161 | 280.862 5, 262.856 4, 96.971 6 | Flavonoids |
| 7 | 7-Hydroxycoumarin | 3.62 | $[M-H]^-$ | $C_9H_6O_3$ | 161.024 | 133.030 0, 123.031 7, 117.034 4, 105.034 7 | Coumarins |
| 8 | 8-Hydroxy-6-methoxy coumarin | 3.66 | $[M-H]^-$ | $C_{10}H_8O_4$ | 191.035 | 176.012 0, 148.016 4, 120.021 6, 104.028 0 | Coumarins |
| 9 | Ferulic acid | 3.82 | $[M-H]^-$ | $C_{10}H_{10}O_4$ | 193.051 | 178.034 7, 134.037 7 | Aromatic organic acids |
| 10 | Vitexin | 3.92 | $[M+H]^+$ | $C_{21}H_{20}O_{10}$ | 433.113 | 415.098 0, 397.088 4, 379.082 2, 367.077 0, 337.066 7, 313.069 3, 283.057 0 | Flavonoids |
| 11 | Baicalein | 4.27 | $[M+H]^+$ | $C_{15}H_{10}O_5$ | 271.060 | 253.095 4, 235.129 7, 225.103 2, 217.155 8, 163.110 1 | Flavonoids |
| 12 | Neodiosmin | 4.58 | $[M+H]^+$ | $C_{28}H_{32}O_{15}$ | 609.181 | 463.120 2 | Flavonoids |
| 13 | Atractyloside I | 4.80 | $[M-H]^-$ | $C_{27}H_{44}O_{13}$ | 575.271 | 397.222 6, 233.065 3, 161.044 4 | Sesquiterpenes |
| 14 | (5*R*,7*R*,10*S*)-Isopterocarpolone *β*-*D*-glucopyranoside | 4.86 | $[M+H]^+$ | $C_{21}H_{34}O_7$ | 399.238 | 331.110 0, 219.172 3 | Sesquiterpenes |
| 15 | (1*S*,5*R*,7*R*,10*R*)-Secoatractylolactone 11-*O*-*β*-*D*-glucopyranoside | 5.02 | $[M-H]^-$ | $C_{21}H_{34}O_{10}$ | 445.208 | 285.039 8 | Sesquiterpenes |
| 16 | Luteolin | 5.92 | $[M-H]^-$ | $C_{15}H_{10}O_6$ | 285.040 | 175.039 5, 151.003 2, 133.029 5, 107.014 1 | Flavonoids |
| 17 | 4*H*-1-Benzopyran-4-one,6-(*β*-*D*-glucopyranosyloxy)-hydroxy-7-methoxy-2-phenyl nuciferine | 6.05 | $[M+H]^+$ | $C_{22}H_{22}O_{10}$ | 447.129 | 285.074 9, 270.050 0 | Flavonoids |
| 18 | (3*Z*,5*E*,11*E*)-3,5,11-Tridecatriene-7,9-diyn-1-yl(2*E*)-3-(4-hydroxy-3-methoxyphenyl)acrylate | 6.06 | $[M+H]^+$ | $C_{23}H_{22}O_4$ | 363.159 | 346.161 3, 328.152 5, 318.166 3, 300.155 5, 274.177 2 | Ester |
| 19 | Atractyloside A | 6.74 | $[M-H]^-$ | $C_{21}H_{36}O_{10}$ | 447.224 | 251.164 5, 159.549 1, 96.970 6 | Sesquiterpenes |
| 20 | 8,9-Epoxy atracolactone | 6.75 | $[M-H]^-$ | $C_{20}H_{36}O_7$ | 387.239 | 256.997 1, 241.001 6, 138.970 8, 96.960 7 | Lactones |
| 21 | Atractylenolide IV | 7.30 | $[M-H]^-$ | $C_{17}H_{22}O_5$ | 305.139 | 261.150 0, 203.107 8, 185.096 4, 174.105 1 | Sesquiterpenes |
| 22 | *trans*-2-Hydroxyisoxypropyl-3-hydroxy-7-isopentene-2,3-dihydrobenzofuran-5-carboxylic acid | 7.57 | $[M+H]^+$ | $C_{17}H_{22}O_5$ | 307.154 | 289.140 4, 247.130 6, 229.117 7, 201.125 3, 187.109 2 | Aromatic organic acids |
| 23 | Diacetyl-atractylodiol | 7.58 | $[M+H]^+$ | $C_{17}H_{20}O_4$ | 289.143 | 229.119 8, 183.112 7, 159.114 7 | Sesquiterpenes |
| 24 | Atractylenolide I | 9.41 | $[M+H]^+$ | $C_{15}H_{18}O_2$ | 231.138 | 213.125 8, 203.138 8, 189.093 2, 185.132 8, 175.076 0, 163.078 5, 161.061 0, 157.100 2, 149.059 4 | Sesquiterpenes |
| 25 | Atractylenolide III | 9.44 | $[M-H]^-$ | $C_{15}H_{20}O_3$ | 247.134 | 229.123 2, 203.145 6, 187.113 2, 147.081 7 | Sesquiterpenes |
| 26 | 1-Acetyl-3-*α*-methylbutyryl-4*E*-6*E*-12*E*-atractytylentriol | 9.78 | $[M-H]^-$ | $C_{21}H_{26}O_5$ | 357.171 | 269.153 3, 87.007 0 | Polyacetylenes |
| 27 | Isoasterolide A | 11.21 | $[M+H]^+$ | $C_{15}H_{20}O_2$ | 233.154 | 215.142 8, 187.148 9, 177.090 7, 159.095 8, 151.077 1 | Steroids |
| 28 | Atractylenolide II | 11.50 | $[M+H]^+$ | $C_{15}H_{20}O_2$ | 233.154 | 215.143 5, 187.151 7, 177.093 5, 159.100 0 | Sesquiterpenes |
| 29 | Anhydroatractylolide | 13.57 | $[M-H]^-$ | $C_{15}H_{22}O_2$ | 233.155 | 120.953 5, 96.969 3 | Sesquiterpenes |
| 30 | Biatractylolide | 19.64 | $[M+H]^+$ | $C_{30}H_{38}O_4$ | 463.284 | 231.137 6, 213.124 2, 175.073 7, 161.058 5, 145.097 0 | Sesquiterpenes |
| 31 | 2-Diene-2,15-dione Linoleic acid | 20.08 | $[M-H]^-$ | $C_{18}H_{32}O_2$ | 279.233 | 261.221 1, 216.900 0, 190.079 4 | Unsaturated fatty acids |

Furthermore, liver tissue staining with H&E and Oil Red O revealed that the Control group exhibited normal histological structures without microvesicular steatosis or lipid droplets; in contrast, the HSHF group showed a marked increase in vacuolar fat degeneration and excessive cytoplasmic lipid droplets (Fig. 2F). Compared to the HSHF group, the amount of vacuolation and number of lipid droplets were significantly reduced in the AMW_L and AMW_H groups. Additionally, liver wet weight and liver TG content were lower in the AMW groups compared to the HSHF group ($P < 0.01$ or $P < 0.05$) (Figs. 2G-J). These results suggest that AMW regulates lipid metabolism in the body.

### *3.3 Impact of AMW on glucose metabolism in mice*

To assess the impact of AMW on glucose metabolism, we first conducted an OGTT. After glucose ingestion, blood glucose levels

significantly increased in all groups at 15 min and remained elevated in the HSHF group at 120 min, while returning to baseline levels in the other groups (Fig. 3A). Corresponding AUC statistics showed that the HSHF group was significantly higher than the Control group ($P < 0.01$), whereas the AMW_H group reduced AUC ($P < 0.05$) (Fig. 3B). Subsequently, serum FBG and FINS levels were measured, and IR and IS indices were calculated. Compared to the Control group, FBG, FINS, and IR levels were significantly elevated ($P < 0.01$), and IS level was reduced in the HSHF group ($P < 0.01$). In contrast, the AMW_L and AMW_H groups showed significantly lower FBG and FINS and IR levels ($P < 0.01$), with increased IS level ($P < 0.01$) (Figs. 3C-F). To further elucidate the effect of AMW on insulin resistance, serum adipokines were measured. Compared to the HSHF group, serum LEP and CHEM levels were significantly reduced ($P < 0.01$), and ADPN and SFRP5 levels were significantly elevated in the treatment groups ($P < 0.01$) (Figs. 3G-J). We also conducted Western blot analysis to measure the levels of IRS2, p-IRS2, and GLUT2 in the liver. Decreased phosphorylation of IRS2 can inhibit normal insulin synthesis and metabolism leading to insulin resistance, while reduced level of GLUT2 can decrease the glucose-sensing ability of pancreatic β-cells, weakening insulin secretion and further exacerbating insulin resistance[32-33]. The HSHF group showed significantly lower p-IRS2/IRS2 and GLUT2 levels compared to the Control group ($P < 0.01$), while AMW_H group was able to reverse ($P < 0.01$ or $P < 0.05$) (Figs. 3K-M). Overall, these experimental results demonstrate that AMW regulates glucose metabolism and improves hepatic insulin resistance.

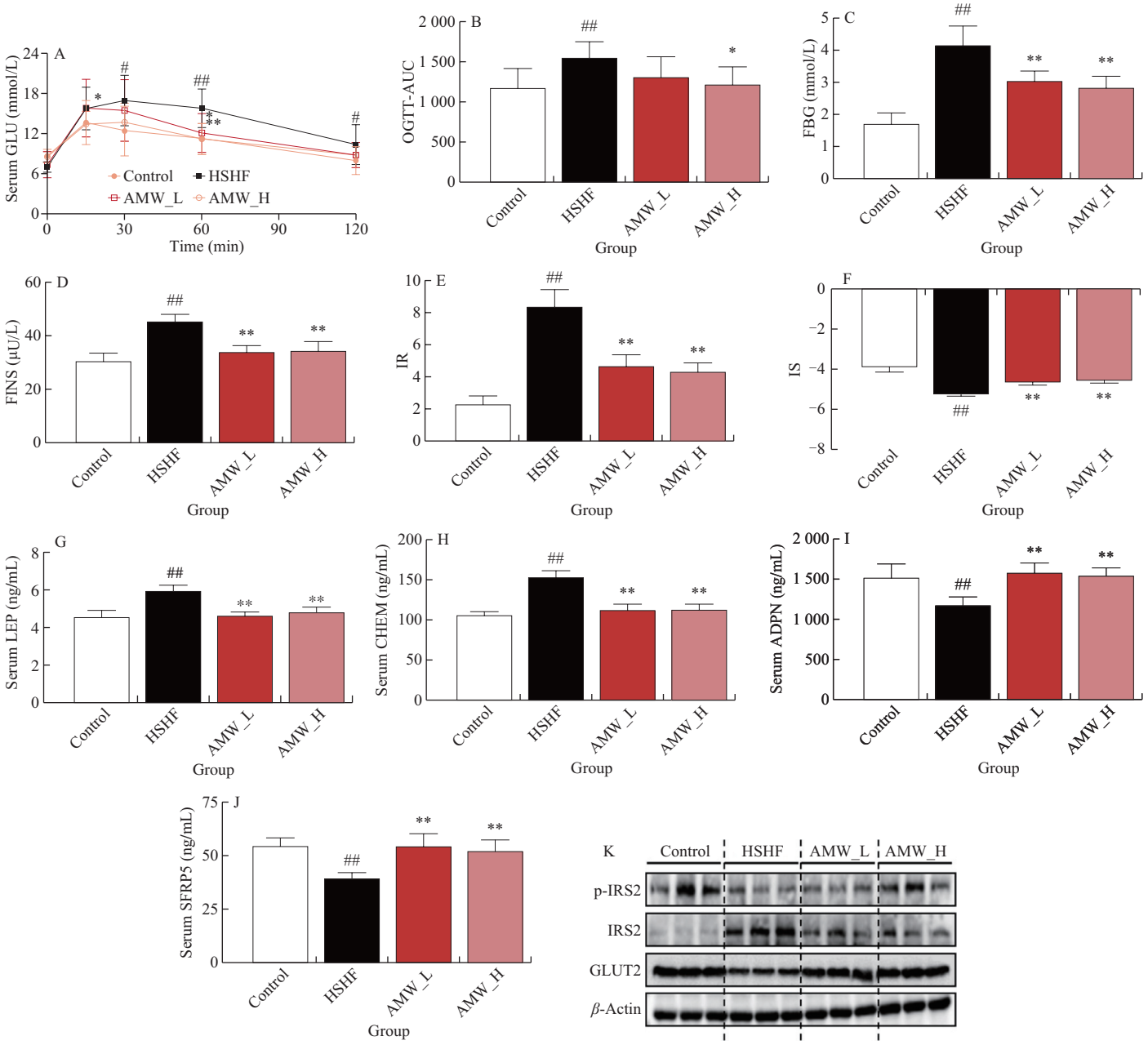



**Fig. 3** AMW modulates glucose metabolism. (A) Serum glucose change curve; (B) OGTT-AUC; Serum levels of (C) FBG, (D) FINS; (E) IR; (F) IS; Serum levels of (G) LEP, (H) CHEM, (I) ADPN, (J) SFRP5 ($n = 8$). (K) Representative images of Western blot for p-IRS2, IRS2, and GULT2 in the liver, with $\beta$-actin as reference; (L) The ratio of p-IRS2/IRS2; (M) The protein levels of GLUT2 ($n = 3$). $^{\#\#}P < 0.01$ compared with the Control group; $^{*}P < 0.05$, $^{**}P < 0.01$ compared with the HSHF group.

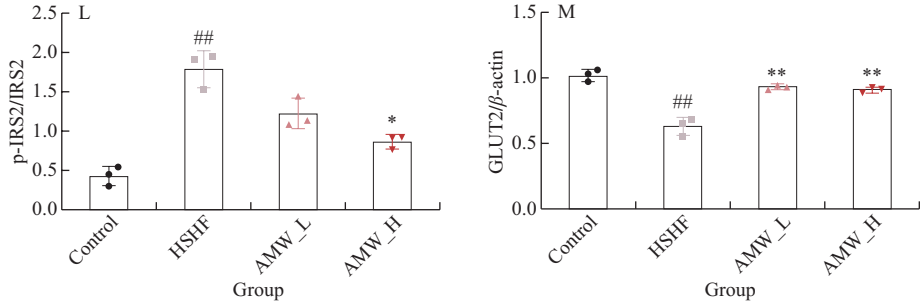



**Fig. 3** (*Continued*)

### *3.4 Impact of AMW on liver function and liver tissue structure in mice*

To assess the impact of AMW on liver function, we measured the serum levels of AST, ALT, ALP, and γ-GT. Compared to the Control group, the HSHF group exhibited significantly elevated levels of serum AST, ALT, ALP, and γ-GT ($P < 0.01$) (Figs. 4A-D). Both AMW_L and AMW_H significantly reduced the levels of these enzymes ($P < 0.01$) (Figs. 4A-D). Additionally, liver tissues were histologically examined using H&E and Masson's trichrome staining to assess the impact of AMW on liver tissue morphology. As shown in Fig. 4E, the HSHF group displayed significant inflammatory cell infiltration, fibrosis, and collagen deposition, while these were markedly reduced in the AMW_L and AMW_H groups. These results indicate that AMW can effectively prevent liver functional damage associated with NAFLD and reduce inflammatory infiltration and collagen deposition between liver cells, preventing liver fibrosis.

### *3.5 Impact of AMW on oxidative stress in mice liver*

To investigate changes in oxidative stress in NAFLD, we first measured serum FFA levels. Compared to the Control group, serum FFA level was significantly increased in the HSHF group ($P < 0.01$), while they were significantly decreased in the AMW_L and AMW_H groups ($P < 0.01$) (Fig. 5A). Using ROS staining, we observed that ROS accumulation in liver tissue was significantly higher in the HSHF group compared to the Control group, whereas it was reduced in the AMW_L and AMW_H groups (Fig. 5B). As shown in Figs. 5C-F, lipid peroxidation appeared to occur in the HSHF group, indicated by decreased SOD activity ($P < 0.01$) and increased levels

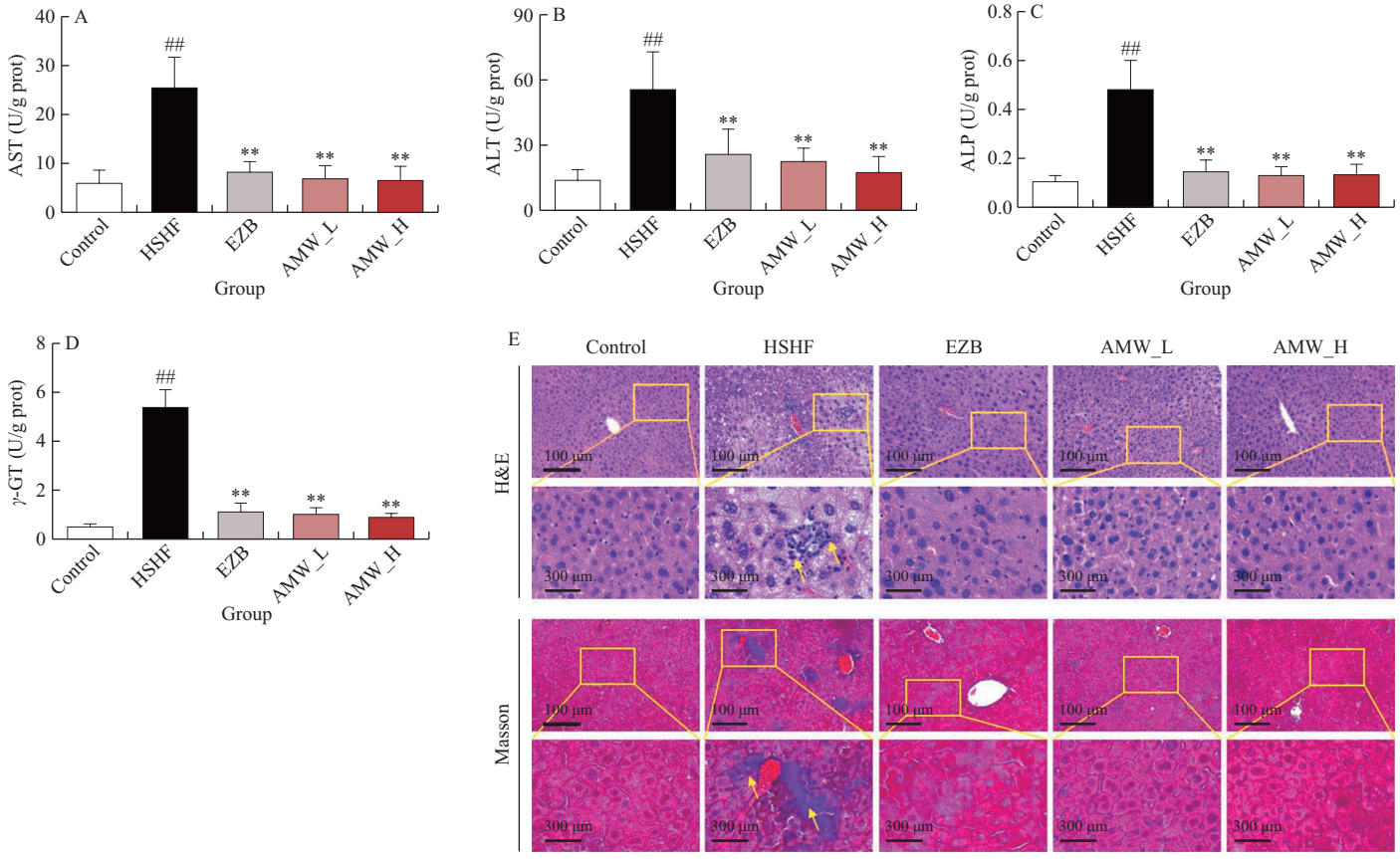



**Fig. 4** AMW improves liver function and liver tissue structure. Liver levels of (A) AST, (B) ALT, (C) ALP, (D) γ-GT ($n = 8$). (E) H&E staining and Masson staining of liver sections (200×, scale bar = 100 μm, yellow arrows indicate inflammatory infiltration or collagen deposition between liver cells). $^{\#}P < 0.05$, $^{\#\#}P < 0.01$ compared with the Control group; $^{*}P < 0.05$, $^{**}P < 0.01$ compared with the HSHF group.

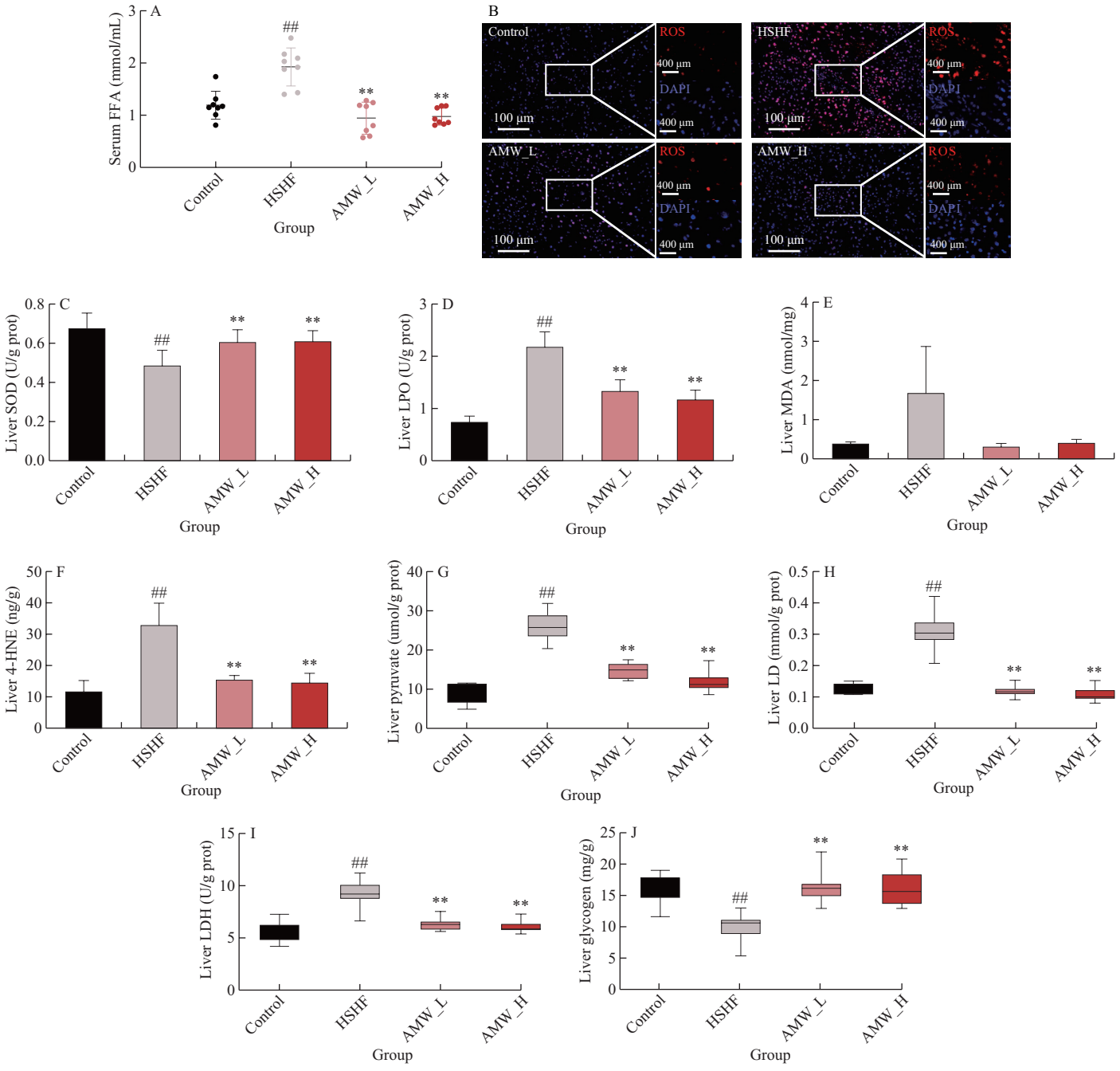



**Fig. 5** AMW improves oxidative stress. (A) Liver level of FFA ($n = 8$). (B) ROS staining of liver sections (200×, scale bar = 100 μm). Liver levels of (C) SOD, (D) LPO, (E) MDA, (F) 4-HNE; Liver level of (G) pyruvate, (H) LD, (I) LDH, (J) Liver glycogen ($n = 8$). $^{\#\#}P < 0.01$ compared with the Control group; $^{*}P < 0.05$, $^{**}P < 0.01$ compared with the HSHF group.

of LPO and 4-HNE compared to the Control group ($P < 0.01$). After administration of different doses of AMW, there was an increase in SOD activity ($P < 0.01$) and a reduction in LPO and 4-HNE levels ($P < 0.01$). Additionally, further evaluation of AMW's effect on liver oxidative stress was performed by measuring liver glycolysis-related markers. Besides a significant increase in liver glycogen content ($P < 0.01$), the levels of pyruvate, LD, and LDH in the liver were significantly reduced in all AMW groups compared to the HSHF group ($P < 0.01$) (Figs. 5G-J). These experimental results suggest that AMW can mitigate liver oxidative stress by reducing serum FFA levels and modulating liver glycolysis.

### *3.6 Impact of AMW on liver inflammation and the TRAF1/ASK1/JNK pathway in mice*

To assess the inflammatory status in the liver, we first measured the levels of IL-1β, IL-6, and TNF-α in the liver homogenate. Compared to the Control group, the HSHF group showed significantly increased levels of IL-1β, IL-6, and TNF-α ($P < 0.01$ or $P < 0.05$), whereas these levels were reduced in all AMW groups compared to the HSHF group ($P < 0.01$ or $P < 0.05$) (Figs. 6A-C). Additionally, immunohisto-chemistry was used to observe the protein level of liver inflammatory factors. As shown in Fig. 6D, compared to the Control group, the levels of IL-1β,

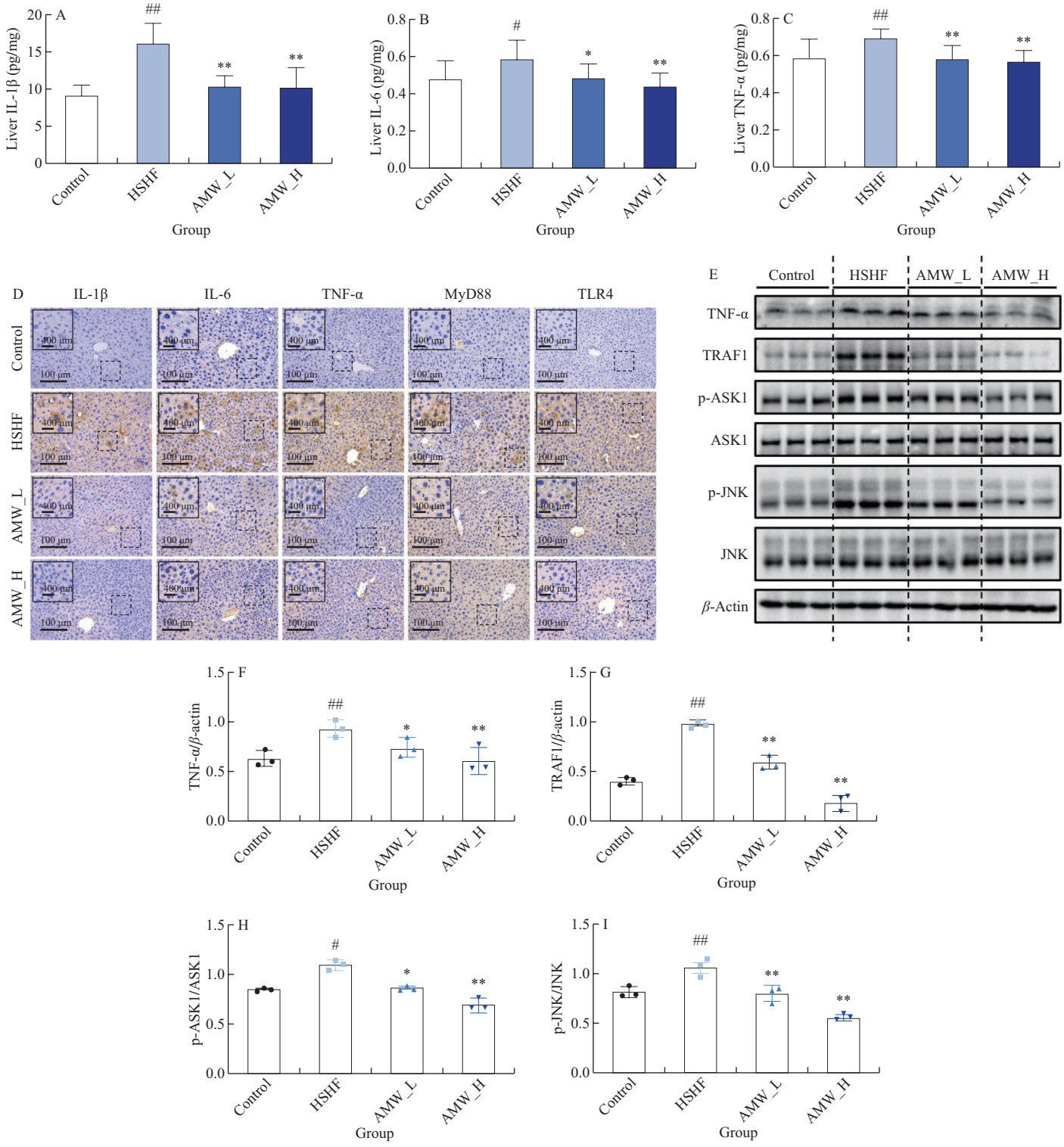



**Fig. 6** AMW improves inflammatory response. Liver levels of (A) IL-1β, (B) IL-6, (C) TNF-α ($n = 8$). (D) Representative images of immunohistochemistry for IL-1β, IL-6, TNF-α, MyD88, and TLR4 (200×, scale bar = 100 μm); (E) Representative images of Western blot for TNF-α, TRAF1, p- ASK1, ASK1, p-JNK, and JNK in the liver, with β-actin as reference; The protein levels of (F) TNF-α, (G) TRAF1; The ratio of (H) p-ASK1/ASK1, (I) p-JNK/JNK ($n = 3$). $^{\#}P < 0.05$, $^{\#\#}P < 0.01$ compared with the Control group; $^{*}P < 0.05$, $^{**}P < 0.01$ compared with the HSHF group.

IL-6, TNF-α, MyD88, and TLR4 were significantly increased in the HSHF group, while AMW groups showed a reduction in the level of these inflammatory markers to varying extents. To further confirm the anti-inflammatory effects of AMW, we analyzed the TRAF1/ASK1/JNK pathway in the liver *via* Western blot, as shown in Figs. 6E-I. All AMW groups could inhibit the levels of TNF-α and TRAF1 and the phosphorylation of ASK1 and JNK ($P < 0.01$ or $P < 0.05$). These results suggest that AMW may modulate the level and production of various inflammatory factors by inhibiting the TRAF1/ASK1/JNK pathway, thereby exerting anti-inflammatory effects.

### 3.7 Impact of AMW on hepatic cell apoptosis in NAFLD mice

After performing TUNEL staining on the liver, we observed that the HSHF group exhibited significantly more hepatic cell apoptosis than the Control group, while all dosages of AMW significantly reduced hepatic cell apoptosis (Fig. 7A), suggesting that AMW can inhibit cell apoptosis triggered by NAFLD. To further confirm the impact of AMW on hepatic cell apoptosis, we analyzed the levels of related apoptotic proteins *via* Western blot. Compared to the Control group, the HSHF group showed significantly increased phosphorylation of AKT ($P < 0.05$) and elevated levels of downstream proteins such as Bax, Cyt C, and Cleaved Caspase-3 ($P < 0.01$), with a significant reduction in Bcl-2 level ($P < 0.01$). However, intervention with AMW_H reversed these changes ($P < 0.01$ or $P < 0.05$) (Figs. 7B-G).

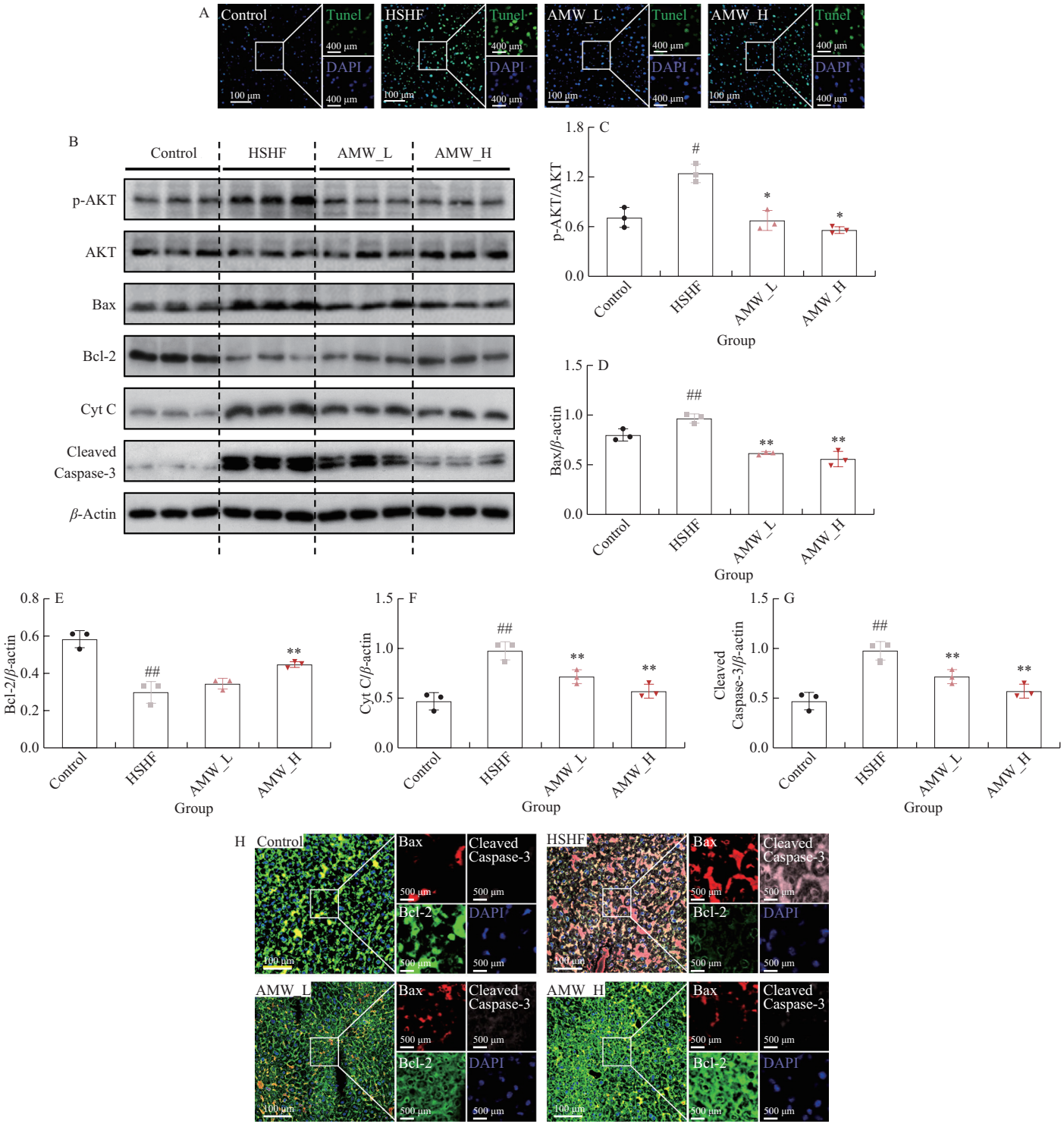



**Fig. 7** AMW inhibits cell apoptosis. (A) TUNEL staining of liver sections (200×, scale bar = 100 μm). (B) Representative images of Western blot for AKT, p-AKT, Bax, Bcl-2, Cyt C, and Cleaved Caspase-3 in the liver, with β-actin as reference. (C) The ratio of p-AKT/AKT. The protein levels of (D) Bax, (E) Bcl-2, (F) Cyt C, (G) Cleaved Caspase-3. (H) Representative images of immunofluorescence for Bax, Bcl-2, and Cleaved Caspase-3 (200×, scale bar = 100 μm). The data were expressed as means ± SD. $^{\#}P < 0.05$, $^{\#\#}P < 0.01$ compared with the Control group; $^{*}P < 0.05$, $^{**}P < 0.01$ compared with the HSHF group; $n = 3$ for each group.

Immunofluorescence was used for further validation, and the levels of Bax, Bcl-2, and Cleaved Caspase-3 proteins in the liver tissues of different groups were consistent with the Western blot results (Fig. 7H). These results indicate that AMW can effectively inhibit cellular apoptosis, thereby preventing liver damage.

## 4. Discussion

In this study, we first analyzed the main components of AMW and found that polysaccharides and lactones are the major components. Among these, *Atractylodes* polysaccharides, atractylenolide I, and atractylenolide III have been proven to have significant pharmacological effects in terms of anti-inflammatory, antioxidant, and lipid deposition inhibition, consistent with our previous predictions[34-36]. Based on these findings, we further investigated the protective effects and mechanisms of AMW on NAFLD induced by HSHF. We observed that AMW could improve disorders of glucose and lipid metabolism, oxidative damage caused by hepatic oxidative stress, and inflammatory injury due to the inflammatory response. Additionally, AMW prevented further exacerbation of hepatic inflammation and hepatocyte apoptosis by inhibiting the TRAF1/ASK1/JNK pathway. These results suggest that AMW can alleviate liver damage by suppressing excessive oxidative stress and inflammation in the liver, thereby reducing apoptosis and preventing further progression of NAFLD. The beneficial effects of AMW may be attributed to the polysaccharides and lactones that it contains.

Liver lipid deposition is one of the primary contributing factors to liver damage in NAFLD[37]. The liver is the central organ for lipid metabolism, and current pharmacological studies often evaluate lipid metabolic function using hepatic lipid indices such as TC, TG, and LDL-C, as well as observing lipid distribution and deposition in the liver through H&E and Oil Red O staining[38-39]. Our experimental results showed that AMW could reduce serum levels of TC, TG, and LDL-C, as well as hepatic TC and TG levels, and decrease ectopic lipid deposition in the liver, indicating that AMW has a beneficial effect on improving liver lipid deposition.

Dysregulation of glucose metabolism is another contributing factor to liver damage in NAFLD[40]. Modern pharmacological research considers glucose tolerance a critical indicator of glucose metabolism, with the liver being a vital organ for maintaining glucose homeostasis[41-42]. Prolonged ingestion of high amounts of glucose by the body will disrupt glucose metabolism homeostasis, leading to elevated levels of insulin in the body. Subsequently, insulin resistance occurs, which further promotes hepatic lipogenesis (Fig. 8)[43]. Aberrant expressions of key factors in the hepatic insulin signaling pathway, such as IRS2 and GLUT2, serve as crucial evaluation indicators for hepatic insulin resistance[44-45]. Further studies have shown that insulin resistance is also associated with adipokines such as LEP, CHEM, ADPN, and SFRP5, which can influence glucose metabolic functions by regulating glucose uptake[46-48]. Experimental results demonstrated that AMW significantly improved glucose tolerance and maintained glucose homeostasis. We also found that AMW regulated the levels of IRS2 and GLUT2 proteins, significantly enhancing insulin sensitivity and markedly reducing insulin resistance levels. Additionally, AMW significantly lowered serum levels of obesity-related factors such as LEP, CHEM, ADPN, and SFRP5. These results suggest that AMW improves glucose metabolic disorders by maintaining glucose stability and suppressing insulin resistance.

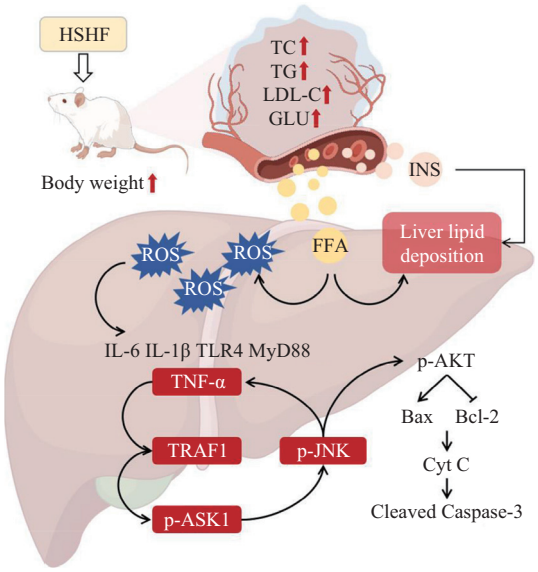



**Fig. 8** Schematic representation of the possible mechanism by which AMW exerts a protective effect against high fat and high sugar diet-induced NAFLD by inhibiting the TRAF1/ASK1/JNK pathway (Image pixel by Figdraw).

Oxidative stress is a key factor in the progression of NAFLD and is closely related to disturbances in glucose and lipid metabolism[49-50]. High serum levels of FFAs are considered alternative markers of impaired lipid metabolism and can directly stimulate excessive production of ROS, thereby initiating oxidative stress mechanisms (Fig. 8)[51-52]. Under conditions of excessive oxidative stress, the activity of SOD is inhibited, further stimulating lipid peroxidation and increasing the levels of lipid peroxidation products such as LPO, MDA, and 4-HNE, ultimately causing oxidative damage[53-54]. Moreover, excessive sugar intake leads to *de novo* lipogenesis in the liver, and the glycolytic process involved can also affect ROS metabolism[55-57]. The quantification of glycolytic activity is customarily achieved through the determination of LD and LDH levels. There is a close correlation between the levels of pyruvate and ROS generated during the glycolytic process. Abnormal accumulation of pyruvate often leads to an increase in ROS levels, thereby causing damage to cells[58-60]. To avoid the potential risks posed by sugar-to-fat conversion, hepatic cells store glucose as glycogen[55]. Our experimental results showed that AMW was able to reduce serum FFA levels and hepatic LD, LDH, and pyruvate contents, increase glycogen content, enhance hepatic SOD activity, reduce hepatic LPO, MDA, and 4-HNE contents, and decrease ROS accumulation in the liver. These findings indicate that AMW can reduce excessive ROS production by lowering serum FFA levels and pyruvate accumulation caused by disturbances in lipid metabolism and glycolysis, thus reducing hepatic oxidative stress and lipid peroxidation, ultimately preventing oxidative damage.

Liver inflammation is a major pathological component of NAFLD and plays a crucial role in the progression of NAFLD from simple steatosis to more severe conditions[61-62]. Studies indicate that ROS-induced lipid peroxidation triggers the extensive release of TNF-α[63]. As the secretion of TNF-α further stimulates the production of other

inflammatory mediators, excessive production of TNF-α leads to over-secretion of inflammatory factors such as MyD88 and TLR4, causing inflammatory damage[64-65]. Additionally, a large amount of TNF-α can act on TRAF1, causing its overexpression, which in turn activates ASK1 phosphorylation, leading to the activation of JNK and inducing the transcription of pro-inflammatory genes such as IL-6, thereby exacerbating inflammatory damage (Fig. 8)[26-28]. Experimental results demonstrated that AMW could reduce the overproduction of TNF-α, decrease the secretion of inflammatory factors such as MyD88 and TLR4, and inhibit the TRAF1/ASK1/JNK pathway, reducing the expression of pro-inflammatory factors IL-6 and IL-1β, thereby preventing further inflammatory damage.

Significant hepatocyte apoptosis is observed in NAFLD, primarily associated with the activation of pro-apoptotic proteins such as Bax[66-67]. Persistent phosphorylation of JNK has been shown to promote the activation of AKT, leading to upregulation of Bax protein levels[68]. Bcl-2 and Bax proteins are antagonistic in the regulation of apoptosis; a high level of Bax protein leads to the formation of Bax/Bax homodimers and inhibits Bax/Bcl-2 heterodimers, thereby promoting apoptosis[69]. Additionally, the binding of Bax to the outer mitochondrial membrane can change mitochondrial permeability, prompting the release of Cyt C from the mitochondria into the cytosol, inducing apoptosis[70]. Once Cyt C is activated, downstream Caspase-3 is activated, triggering a caspase cascade and directly cleaving protein substrates, thereby leading to apoptosis (Fig. 8)[71-72]. Our experimental results showed that AMW could inhibit the levels of liver proteins such as AKT, Bax, Cyt C, and Cleaved Caspase-3, while promoting the level of Bcl-2 in the liver, indicating that AMW has a protective effect against hepatocyte apoptosis.

## 5. Conclusion

In summary, this study demonstrates that AMW can exert a protective effect on NAFLD by improving hepatic glucose and lipid metabolism, inhibiting oxidative stress and the TRAF1/ASK1/JNK signaling pathway, reducing inflammation, and preventing apoptosis. Therefore, the findings suggest that the water extract of *A. macrocephala* may be an effective dietary supplement for improving NAFLD and preventing its further deterioration. Furthermore, the major active components contributing to these effects are likely the polysaccharides and lactones present in AMW.

## Declaration of competing interest

The authors declare no competing financial interests.

## Acknowledgments

This study was supported by the National Natural Science Foundation China (82003977), the Zhejiang Provincial Natural Science Foundation (LY24H280004), the Zhejiang research and development program (2020C04020).

### References

[1] A. Hokkanen, H. Hämäläinen, T.M. Laitinen, et al., Test-retest reliability of the assessment of fatty liver disease using low-dose computed tomography in cardiac patients, Front. Med. 8 (2021) 656658. https://doi.org/10.3389/fmed.2021.656658.

[2] E. Grossini, D.P. Garhwal, G. Calamita, et al., Exposure to plasma from non-alcoholic fatty liver disease patients affects hepatocyte viability, generates mitochondrial dysfunction, and modulates pathways involved in fat accumulation and inflammation, Front. Med. 8 (2021) 693997. https://doi.org/10.3389/fmed.2021.693997.

[3] W. Kopp, How western diet and lifestyle drive the pandemic of obesity and civilization diseases, Diabetes, Metab. Syndr. Obes. 12 (2019) 2221-2236. https://doi.org/10.2147/DMSO.S216791.

[4] L. Rong, J. Zou, W. Ran, et al., Advancements in the treatment of non-alcoholic fatty liver disease (NAFLD), Front. Endocrinol. 13 (2023) 1087260. https://doi.org/10.3389/fendo.2022.1087260.

[5] Y. Zou, Z. Chen, C. Sun, et al., Exercise intervention mitigates pathological liver changes in NAFLD zebrafish by activating SIRT1/AMPK/NRF2 signaling, Int. J. Mol. Sci. 22 (2021) 10940. https://doi.org/10.3390/ijms222010940.

[6] J.W. Guo, X. Liu, T.T. Zhang, et al., Hepatocyte TMEM16A deletion retards NAFLD progression by ameliorating hepatic glucose metabolic disorder, Adv. Sci. 7 (2020) 1903657. https://doi.org/10.1002/advs.201903657.

[7] M.C. Podszun, A.S. Alawad, S. Lingala, et al., Vitamin E treatment in NAFLD patients demonstrates that oxidative stress drives steatosis through upregulation of *de-novo* lipogenesis, Redox. Biol. 37 (2020) 101710. https://doi.org/10.1016/j.redox.2020.101710.

[8] S. Gómez-Zorita, M. González-Arceo, J. Trepiana, et al., Comparative effects of pterostilbene and its parent compound resveratrol on oxidative stress and inflammation in steatohepatitis induced by high-fat high-fructose feeding, Antioxidants 9 (2020) 1042. https://doi.org/10.3390/antiox9111042.

[9] J. Li, T. Wang, P. Liu, et al., Hesperetin ameliorates hepatic oxidative stress and inflammation *via* the PI3K/AKT-Nrf2-ARE pathway in oleic acid-induced HepG2 cells and a rat model of high-fat diet-induced NAFLD, Food Funct. 12 (2021) 3898-3918. https://doi.org/10.1039/d0fo02736g.

[10] W. Ke, P. Wang, X. Wang, et al., Dietary platycodon grandiflorus attenuates hepatic insulin resistance and oxidative stress in high-fat-diet induced non-alcoholic fatty liver disease, Nutrients 12 (2020) 480. https://doi.org/10.3390/nu12020480.

[11] M.M.H. Tusher, M. Asrafuzzaman, M.H. Rahman, et al., Effects of *Dillenia indica* L. fruit extract on hepatic *Cyp7a1* gene expression in a rat model of streptozotocin-induced diabetes-associated dyslipidemia, CTMP 7 (2026) 200289. https://doi.org/10.1016/j.ctmp.2026.200289.

[12] O.V. Chernikov, H.W. Chiu, L.H. Li, et al., Immunomodulatory properties of polysaccharides from the coral *Pseudopterogorgia americana* in macrophages, Cells 10 (2021) 3531. https://doi.org/10.3390/cells10123531.

[13] B. Wan, M. Xue, W.X. Chen, TRAF1 meditates lipopolysaccharide-induced acute lung injury by up regulating JNK activation, Biochem. Biophys. Res. Commun. 511 (2019) 49-56. https://doi.org/10.1016/j.bbrc.2019.01.041.

[14] W. Xu, L. Zhang, Y. Zhang, et al., TRAF1 exacerbates myocardial ischemia reperfusion injury *via* ASK1-JNK/p38 signaling, J. Am. Heart. Assoc. 8 (2019) e012575. https://doi.org/10.1161/JAHA.119.012575.

[15] H. Zhu, L. Zhang, H. Jia, et al., Tetrahydrocurcumin improves lipopolysaccharide-induced myocardial dysfunction by inhibiting oxidative stress and inflammation *via* JNK/ERK signaling pathway regulation, Phytomedicine 104 (2022) 154283. https://doi.org/10.1016/j.phymed.2022.154283.

[16] A. John, H. Raza. Azadirachtin attenuates lipopolysaccharide-induced ROS production, DNA damage, and apoptosis by regulating JNK/Akt and AMPK/mTOR-dependent pathways in Rin-5F pancreatic beta cells, Biomedicines 9 (2021) 1943. https://doi.org/10.3390/biomedicines9121943.

[17] C. Liang, Y. Ma, L. Yong, et al., Y-box binding protein-1 promotes tumorigenesis and progression *via* the epidermal growth factor receptor/AKT pathway in spinal chordoma, Cancer Sci. 110 (2019) 166-179. https://doi.org/10.1111/cas.13875.

[18] S. Munakarmi, L. Chand, H.B. Shin, et al., Indole-3-carbinol derivative DIM mitigates carbon tetrachloride-induced acute liver injury in mice by inhibiting inflammatory response, apoptosis and regulating oxidative stress, Int. J. Mol. Sci. 21 (2020) 2048. https://doi.org/10.3390/ijms21062048.

[19] C. Guo, Q. Li, R. Chen, et al., Baicalein alleviates non-alcoholic fatty liver disease in mice by ameliorating intestinal barrier dysfunction, Food Funct. 14 (2023) 2138-2148. https://doi.org/10.1039/d2fo03015b.

[20] Z.J. Liu, J. Zhong, M. Zhang, et al., The alexipharmic mechanisms of five licorice ingredients involved in CYP450 and Nrf2 pathways in paraquat-induced mice acute lung injury, Oxid. Med. Cell. Longev. 2019 (2019) 7283104. https://doi.org/10.1155/2019/7283104.

[21] J.M. Yang, Y. Sun, M. Wang, et al., Regulatory effect of a Chinese herbal medicine formula on non-alcoholic fatty liver disease, World. J. Gastroenterol. 25 (2019) 5105-5119. https://doi.org/10.3748/wjg.v25.i34.5105.

[22] J. Sun, H. Luo, Y. Jiang, et al., Influence of nutrient (NPK) factors on growth, and pharmacodynamic component biosynthesis of atractylodes chinensis: an insight on acetyl-CoA carboxylase (ACC), 3-hydroxy-3-methylglutaryl-CoA reductase (HMGR), and farnesyl pyrophosphate synthase (FPPS) signaling responses, Front. Plant. Sci. 13 (2022) 799201. https://doi.org/10.3389/fpls.2022.799201.

[23] R. Bo, X. Liu, J. Wang, et al., Polysaccharide from *Atractylodes macrocephala* Koidz binding with zinc oxide nanoparticles: characterization, immunological effect and mechanism, Front. Nutr. 9 (2022) 992502. https://doi.org/10.3389/fnut.2022.992502.

[24] C.F. Chau, S.H. Wu, The development of regulations of Chinese herbal medicines for both medicinal and food uses, Trends Food. Sci. Tech. 17 (2006) 313-323. https://doi.org/10.1016/j.tifs.2005.12.005.

[25] Y. Wu, H. Meng, B. Qiao, et al., Yifei Sanjie formula treats chronic obstructive pulmonary disease by remodeling pulmonary microbiota, Front. Med. 9 (2022) 927607. https://doi.org/10.3389/fmed.2022.927607.

[26] H.L. Kim, S.K. Lee, D.E. Min, et al., Anti-Obesity effects of a mixture of *Atractylodes macrocephala* and *Amomum villosum* extracts on 3T3-L1 adipocytes and high-fat diet-induced obesity in mice, Molecules 27 (2022) 906. https://doi.org/10.3390/molecules27030906.

[27] B. Zhang, L. Hong, J. Ke, et al., Polysaccharide of *Atractylodes macrocephala* Koidz alleviate lipopolysaccharide-induced liver injury in goslings *via* the p53 and FOXO pathways, Poult. Sci. 102 (2023) 102480. https://doi.org/10.1016/j.psj.2023.102480.

[28] Y. Li, T. Sun, Y. Hong, et al., Mixture of five fermented herbs (Zhihuasi Tk) alters the intestinal microbiota and promotes the growth performance in piglets, Front. Microbiol. 12 (2021) 725196. https://doi.org/10.3389/fmicb.2021.725196.

[29] M. Gu, Z. Chen, Y. Chen, et al., Unlocking the potential of atractylenolide II: Mitigating non-alcoholic fatty liver disease through farnesoid X receptor-endoplasmic reticulum stress interplay, J. Pharm. Anal. 15 (2025) 101318. https://doi.org/10.1016/j.jpha.2025.101318.

[30] Z. Xie, M. Lin, X. He, et al., Chemical constitution, pharmacological effects and the underlying mechanism of atractylenolides: a review, Molecules 28 (2023) 3987. https://doi.org/10.3390/molecules28103987.

[31] Y. Jiang, K. Guo, P. Wang, et al., The antitumor properties of atractylenolides: molecular mechanisms and signaling pathways, Biomed. Pharmacother. 155 (2022) 113699. https://doi.org/10.1016/j.biopha.2022.113699.

[32] K. Enooku, M. Kondo, N. Fujiwara, et al., Hepatic IRS1 and $\beta$-catenin expression is associated with histological progression and overt diabetes emergence in NAFLD patients, J. Gastroenterol. 53 (2018) 1261-1275. https://doi.org/10.1007/s00535-018-1472-0.

[33] G. Tomar, M. Singh, I. Sharma, et al., Metformin reduces testosterone level in type 2 diabetes mellitus patients and its therapy by traditional medicine, CTMP 5 (2024) 200167. https://doi.org/10.1016/j.ctmp.2024.200167.

[34] X. Xiang, N. Cao, F. Chen, et al., Polysaccharide of *Atractylodes macrocephala* Koidz (PAMK) alleviates cyclophosphamide-induced immunosuppression in mice by upregulating CD28/IP3R/PLCγ-1/AP-1/NFAT signal pathway, Front. Pharmacol. 11 (2020) 529657. https://doi.org/10.3389/fphar.2020.529657.

[35] H. Xu, K. Van der Jeught, Z. Zhou, et al., Atractylenolide I enhances responsiveness to immune checkpoint blockade therapy by activating tumor antigen presentation, J. Clin. Invest. 131 (2021) e146832. https://doi.org/10.1172/JCI146832.

[36] J. Han, W. Li, G. Shi, et al., Atractylenolide III improves mitochondrial function and protects against ulcerative colitis by activating AMPK/SIRT1/PGC-1α, Mediators Inflamm. 2022 (2022) 9129984. https://doi.org/10.1155/2022/9129984.

[37] F.Z. Xin, Z.H. Zhao, R.N. Zhang, et al., Folic acid attenuates high-fat diet-induced steatohepatitis *via* deacetylase SIRT1-dependent restoration of PPARα, World J. Gastroenterol. 26 (2020) 2203-2220. https://doi.org/10.3748/wjg.v26.i18.2203.

[38] K. Luo, W. Huang, L. Qiao, et al., *Dendrocalamus latiflorus* and its component rutin exhibit glucose-lowering activities by inhibiting hepatic glucose production *via* AKT activation, Acta. Pharm. Sin. B 12 (2022) 2239-2251. https://doi.org/10.1016/j.apsb.2021.11.017.

[39] N. Wu, F. Yuan, S. Yue, et al., Effect of exercise and diet intervention in NAFLD and NASH *via* GAB2 methylation, Cell. Biosci. 11 (2021) 189. https://doi.org/10.1186/s13578-021-00701-6.

[40] M. Rebollo-Hernanz, Y. Aguilera, M.A. Martin-Cabrejas, et al., Phytochemicals from the cocoa shell modulate mitochondrial function, lipid and glucose metabolism in hepatocytes *via* activation of FGF21/ERK, AKT, and mTOR pathways, Antioxidants 11 (2022) 136. https://doi.org/10.3390/antiox11010136.

[41] R. Czapiewski, D.G. Batrakou, J.I. de Las Heras, et al., Genomic loci mispositioning in *Tmem120a* knockout mice yields latent lipodystrophy, Nat. Commun. 13 (2022) 321. https://doi.org/10.1038/s41467-021-27869-2.

[42] X. Xiao, P. Qiu, H.Z. Gong, et al., PACAP ameliorates hepatic metabolism and inflammation through up-regulating FAIM in obesity, J. Cell. Mol. Med. 23 (2019) 5970-5980. https://doi.org/10.1111/jcmm.14453.

[43] Y. Zhao, Q.Y. Wang, L.T. Zeng, et al., Long-term high-fat high-fructose diet induces type 2 diabetes in rats through oxidative stress, Nutrients 14 (2022) 2181. https://doi.org/10.3390/nu14112181.

[44] Y. Takayanagi, K. Ishizuka, T.M. Laursen, et al., From population to neuron: exploring common mediators for metabolic problems and mental illnesses, Mol. Psychiatry. 26 (2021) 3931-3942. https://doi.org/10.1038/s41380-020-00939-5.

[45] N. Rao, X. Wang, Y. Zhai, et al., Stem cells from human exfoliated deciduous teeth ameliorate type II diabetic mellitus in Goto-Kakizaki rats, Diabetol. Metab. Syndr. 11 (2019) 22. https://doi.org/10.1186/s13098-019-0417-y.

[46] X. Wang, T. Xu, R. Liu, et al., High-fiber diet or combined with acarbose alleviates heterogeneous phenotypes of polycystic ovary syndrome by regulating gut microbiota, Front. Endocrinol. 12 (2022) 806331. https://doi.org/10.3389/fendo.2021.806331.

[47] K. Boonloh, V. Kukongviriyapan, B. Kongyingyoes, et al., Rice bran protein hydrolysates improve insulin resistance and decrease pro-inflammatory cytokine gene expression in rats fed a high carbohydrate-high fat diet, Nutrients 7 (2015) 6313-6329. https://doi.org/10.3390/nu7085292.

[48] D.M. Schulte, D. Kragelund, N. Müller, et al., The wingless-related integration site-5a/secreted frizzled-related protein-5 system is dysregulated in human sepsis, Clin. Exp. Immunol. 180 (2015) 90-97. https://doi.org/10.1111/cei.12484.

[49] J. An, L. Cheng, L. Yang, et al., P-Hydroxybenzyl alcohol alleviates oxidative stress in a nonalcoholic fatty liver disease larval zebrafish model and a BRL-3A hepatocyte *via* the Nrf2 pathway, Front. Pharmacol. 12 (2021) 646239. https://doi.org/10.3389/fphar.2021.646239.

[50] Y. Zhang, Y. Li, J. Zhao, et al., Protective effects and mechanisms of polyethylene glycol loxenatide against hyperglycemia and liver injury in *db/db* diabetic mice, Front. Pharmacol. 12 (2021) 781856. https://doi.org/10.3389/fphar.2021.781856.

[51] P. Posadas-Rodríguez, N.E. Posadas-Rodríguez, V.Y. González-Puertos, et al., tBHQ induces a hormetic response that protects L6 myoblasts against the toxic effect of palmitate, Oxid. Med. Cell. Longev. 2020 (2020) 3123268. https://doi.org/10.1155/2020/3123268.

[52] Q.Q. Liu, K. Ren, S.H. Liu, et al., MicroRNA-140-5p aggravates hypertension and oxidative stress of atherosclerosis via targeting Nrf2 and Sirt2, Int. J. Mol. Med. 43 (2019) 839-849. https://doi.org/10.3892/ijmm.2018.3996.

[53] W. Zheng, Z. Song, S. Li, et al., Protective effects of sesamol against liver oxidative stress and inflammation in high-fat diet-induced hepatic steatosis, Nutrients 13 (2021) 4484. https://doi.org/10.3390/nu13124484.

[54] M. Liu, C. Sun, X. Zheng, et al., Comparative proteomic analysis revealed the mechanism of tea tree oil targeting lipid metabolism and antioxidant system to protect hepatopancreatic health in *Macrobrachium rosenbergii*, Front. Immunol. 13 (2022) 906435. https://doi.org/10.3389/fimmu.2022.906435.

[55] H.V. Lin, Y.C. Tsou, Y.T. Chen, et al., Effects of low-molecular-weight fucoidan and high stability fucoxanthin on glucose homeostasis, lipid metabolism, and liver function in a mouse model of type II diabetes, Mar Drugs 15(2017) 113. https://doi.org/10.3390/md15040113.

[56] Z. Ma, H.Wang, Y. Cai, et al., Epigenetic drift of H3K27me3 in aging links glycolysis to healthy longevity in *Drosophila*, eLife 7 (2018) e35368. https://doi.org/10.7554/eLife.35368.

[57] H.A. Alkhatabi, S.F. Zohny, M.R. Shait Mohammed, et al., Venetoclax-resistant MV4-11 leukemic cells activate PI3K/AKT pathway for metabolic reprogramming and redox adaptation for survival, Antioxidants 11 (2022) 461. https://doi.org/10.3390/antiox11030461.

[58] S. Yang, L.H. Long, D. Li, et al., *β*-Guanidinopropionic acid extends the lifespan of *Drosophila melanogaster via* an AMP-activated protein kinase-dependent increase in autophagy, Aging Cell 14 (2015) 1024-1033. https://doi.org/10.1111/acel.12371.

[59] M.P. Thelen, B. Wirth, M.J. Kye. Mitochondrial defects in the respiratory complex I contribute to impaired translational initiation *via* ROS and energy homeostasis in SMA motor neurons, Acta. Neuropathol. Commun. 8 (2020) 223. https://doi.org/10.1186/s40478-020-01101-6.

[60] C. Wu, X. Zhang, W. Fang, Increasing pyruvate concentration enhances conidial thermotolerance in the entomopathogenic fungus *Metarhizium robertsii*, Front. Microbiol. 10 (2019) 519. https://doi.org/10.3389/fmicb.2019.00519.

[61] X. Li, J. Wang, X. Gong, et al., Upregulation of BCL-2 by acridone derivative through gene promoter I-motif for alleviating liver damage of NAFLD/NASH, Nucleic. Acids Res. 48 (2020) 8255-8268. https://doi.org/10.1093/nar/gkaa615.

[62] C. Huang, X. Wei, Q. Luo, et al., Loss of TRIM67 attenuates the progress of obesity-induced non-alcoholic fatty liver disease, Int. J. Mol. Sci. 23 (2022) 7475. https://doi.org/10.3390/ijms23137475.

[63] J.P. Yang, J.H. Shin, S.H. Seo, et al., Effects of antioxidants in reducing accumulation of fat in hepatocyte, Int. J. Mol. Sci. 19 (2018) 2563. https://doi.org/10.3390/ijms19092563.

[64] N. Dong, X. Xu, C. Xue, et al., Ethyl pyruvate inhibits LPS induced IPEC-J2 inflammation and apoptosis through p38 and ERK1/2 pathways, Cell Cycle 18 (2019) 2614-2628. https://doi.org/10.1080/15384101.2019.1653106.

[65] F.M. Davis, A. denDekker, A.D. Joshi, et al., Palmitate-TLR4 signaling regulates the histone demethylase, JMJD3, in macrophages and impairs diabetic wound healing, Eur. J. Immunol. 50 (2020) 1929-1940. https://doi.org/10.1002/eji.202048651.

[66] M. Jiang, C. Li, Q. Liu, et al., Inhibiting ceramide synthesis attenuates hepatic steatosis and fibrosis in rats with non-alcoholic fatty liver disease, Front. Endocrinol. 10 (2019) 665. https://doi.org/10.3389/fendo.2019.00665.

[67] N. Choi, J.W. Kim, H. Jeong, et al., Fermented ginseng, GBCK25, ameliorates steatosis and inflammation in nonalcoholic steatohepatitis model, J. Ginseng Res. 43 (2019) 196-208. https://doi.org/10.1016/j.jgr.2017.10.002.

[68] Y. Gao, K. Ma, Z. Zhu, et al., Modified Erchen decoction ameliorates cognitive dysfunction in vascular dementia rats *via* inhibiting JAK2/STAT3 and JNK/BAX signaling pathways, Phytomedicine 114 (2023) 154797. https://doi.org/10.1016/j.phymed.2023.154797.

[69] Y. Yang, X. Du, Q. Wang, et al., Mechanism of cell death induced by silica nanoparticles in hepatocyte cells is by apoptosis, Int. J. Mol. Med. 44 (2019) 903-912. https://doi.org/10.3892/ijmm.2019.4265.

[70] A. Chen, H. Wang, Y. Zhang, et al., Paeoniflorin exerts neuroprotective effects against glutamate-induced PC12 cellular cytotoxicity by inhibiting apoptosis, Int. J. Mol. Med. 40 (2017) 825-833. https://doi.org/10.3892/ijmm.2017.3076.

[71] Z. Cao, S. Wang, M. Qi, et al., Exploring the induction of endometrial epithelial cell apoptosis in clinical-type endometritis in yaks through the Cyt-c/caspase-3 signaling axis, Microb. Pathog. 18 (2024) 106470. https://doi.org/10.1016/j.micpath.2023.106470.

[72] Y. Wang, X. Chang, B. Zheng, et al., Protective effect of *Ganoderma atrum* polysaccharide on acrolein-induced apoptosis and autophagic flux in IEC-6 cells, Foods 11 (2022) 240. https://doi.org/10.3390/foods11020240.